

---

# Notes on bias and covariance matrix of the angular power spectrum on small sky maps

---

C. Magneville and J.P. Pansart

DSM/DAPNIA , CEA/SACLAY , F-91191 Gif-sur-Yvette.

*Abstract:*

We compute the effects induced by the use of small CMB maps on the measurement of the  $C_l$  coefficients of the angular power spectrum and show that small systematic effects have to be taken into account. We also compute numerically the cosmic variance and covariance of the  $C_l$  spectrum for various spherical cap like maps. Comparisons with simulations are presented. The calculations are done using the standard method based on the spherical harmonic transform or using the temperature angular correlation spectrum.



# Contents

I	Introduction . . . . .	1
II	Estimating the power spectrum: formalism for the full sphere. . . . .	2
	ii.1 Spectrum and angular correlation fonction definition. . . . .	2
	ii.2 Power spectrum estimator. . . . .	3
	ii.3 Angular correlation function estimator. . . . .	4
	ii.4 What about computing the $C_l$ on a portion of sphere? . . . . .	5
III	Spectrum estimation for a portion of sphere. . . . .	8
	iii.1 Estimator of the $C_l$ spectrum. . . . .	8
	iii.2 Computation of the bias of the estimator. . . . .	8
	iii.3 Computation of the covariance of the $\tilde{C}_l$ estimator for spherical cap maps. . . . .	11
	iii.4 Discussion and comparison with simulations . . . . .	14
IV	Angular correlation function estimation for a portion of sphere. . . . .	27
	iv.1 Estimator of the angular correlation function. . . . .	27
	iv.2 Comparison of the estimator with the $\langle \tilde{C}_l \rangle$ . . . . .	28
	iv.3 Covariance of the estimator of the angular correlation function on partial map. . . . .	29
V	$C_l$ estimation using the angular correlation function for a portion of sphere. . . . .	32
	v.1 Using integration of the angular correlation function. . . . .	32
	v.2 Using integration of a smooth apodization of the angular correlation function. . . . .	33
	v.3 Practical $C_l$ reconstruction from the angular correlation spectrum. . . . .	36
VI	Conclusion. . . . .	45
<b>APPENDICES:</b>		<b>46</b>
A	Computation of the angular correlation integral. . . . .	46
B	Computation of the $\tilde{C}_l$ covariance for a portion of sphere. . . . .	48
C	Computation of the angular correlation distribution for a portion of sphere. . . . .	51

D	Computation of the angular correlation integral for a portion of sphere. . . . .	54
	<b>Bibliography.</b>	<b>55</b>

# I Introduction

The field of cosmic microwave background (CMB) anisotropies has dramatically advanced over the last decade especially on its observational front. Satellite experiments (COBE,WMAP) observed the whole sky. But to study the high multipoles of the power spectrum, balloon-borne experiments have emerged.

The BOOMERANG ([De Bernardis et al, 2000]), the MAXIMA ([Hanany et al, 2000]) and the ARCHEOPS ([Benoit et al, 2003]) balloon experiments made measurements of the first doppler peak of the CMB spectrum. Due to a limited observing time and technical constraints, these experiments only observed a small fraction of the sky. BOOMERANG observed a region of  $1800 \text{ deg}^2$  and measured the spectrum up to multipoles  $l_{max} \sim 1000$  and MAXIMA observed  $124 \text{ deg}^2$  and measured the spectrum up to  $l_{max} \sim 785$ . In the future, the OLIMPO experiment ([Masi et al, 2006]) will observe  $300 \text{ deg}^2$  and measure the spectrum up to  $l_{max} \sim 2500$ .

In this paper we compute the effects induced by the use of small CMB maps on the measurement of the  $C_l$  spectrum at high multipole moments. Two methods are used to compute the  $C_l$  coefficients. The first one uses the Fast Fourier Transform (FFT) technics and the second one the angular correlation spectrum. These two technics are complementary and lead to different biases. We show how the variance behaves with respect to the map size and how the apodization works in the case of the angular correlation spectrum. These calculations will be compared with simulated CMB maps of various sizes and shapes. Numerical calculations provide a fast tool to assess most of the biases.

## II Estimating the power spectrum: formalism for the full sphere.

### ii.1 Spectrum and angular correlation fonction definition.

The observed temperature  $T$  on the 2-sphere is a random field that can be expanded on the spherical harmonic basis:

$$T(\theta, \phi) = \sum_{l=0}^{\infty} \sum_{m=-l}^{+l} a_{lm} Y_l^m(\theta, \phi) \quad (\text{II.1})$$

where the  $a_{lm}$  coefficients are random variables. With  $\vec{\Omega} \equiv (\theta, \phi)$  one has<sup>1</sup>

$$a_{lm} = \int_{S^2} T(\vec{\Omega}) \overline{Y_l^m(\vec{\Omega})} d\vec{\Omega} \quad (\text{II.2})$$

$T(\vec{\Omega})$  is a real field so  $\overline{a_{l-m}} = (-1)^m a_{lm}$  which is a consequence of the relation  $\overline{Y_l^{-m}} = (-1)^m Y_l^m$ .

The observed sky is a particular realisation of that random field. If one assumes uncorrelated  $a_{lm}$  coefficients and isotropy, one has:

$$\langle \overline{a_{lm}} a_{l'm'} \rangle_{ens} = \delta_{ll'} \delta_{mm'} C_l \quad (\text{II.3})$$

where the  $C_l$  are specified by the cosmological theory and the symbol  $\langle \rangle_{ens}$  means averaging over many sky realisations.

The temperature angular correlation function is defined as:

$$\xi(\vec{\Omega}, \vec{\Omega}') = \langle T(\vec{\Omega}) T(\vec{\Omega}') \rangle_{ens} \quad (\text{II.4})$$

where  $\vec{\Omega}, \vec{\Omega}'$  are the directions of measurement. The temperature angular correlation function is related to the spectrum of the primordial fluctuations. With the isotropy hypothesis, the angular correlation function is only a function of the angular separation  $\gamma$  with  $\cos(\gamma) = \vec{\Omega} \cdot \vec{\Omega}'$ . We have:

$$\begin{aligned} \xi(\gamma) &= \langle \overline{T(\Omega)} T(\Omega') \rangle_{ens} \\ &= \sum_{l,m} \sum_{l',m'} \langle \overline{a_{lm}} a_{l'm'} \rangle_{ens} \overline{Y_l^m(\Omega)} Y_{l'}^{m'}(\Omega') \\ &= \sum_{l,m} \sum_{l',m'} C_l \delta_{ll'} \delta_{mm'} \overline{Y_l^m(\Omega)} Y_{l'}^{m'}(\Omega') \\ &= \sum_{l,m} C_l \overline{Y_l^m(\Omega)} Y_l^m(\Omega') \\ &= \frac{1}{4\pi} \sum_l (2l+1) C_l P_l(\cos(\gamma)) \end{aligned}$$

This relation can be inverted and finally:

---

<sup>1</sup>The overbar means complex conjugation

$$\xi(\gamma) = \frac{1}{4\pi} \sum_{l=0}^{\infty} (2l+1) C_l P_l(\cos(\gamma)) \quad (\text{II.5})$$

$$C_l = 2\pi \int_{\gamma=0}^{\pi} \xi(\gamma) P_l(\cos(\gamma)) d \cos(\gamma)$$

In the rest of these notes, the isotropy hypothesis (II.3) will always be assumed.

## ii.2 Power spectrum estimator.

In practice, one observes a unique sky realisation and estimators of the power spectrum and the angular correlation function have to be constructed: instead of averaging over many sky realisations, we can use the sky isotropy hypothesis. The bias and variance of such estimators have to be computed.

We can have an estimation of the  $a_{lm}$  by using (II.2). Then we get an estimator  $\widehat{C}_l$  of the  $C_l$  spectrum by averaging over  $m$ :

$$\widehat{C}_l = \frac{1}{2l+1} \sum_{m=-l}^l |a_{lm}|^2 \quad (\text{II.6})$$

For the whole sky, this estimator is unbiased:

$$\langle \widehat{C}_l \rangle_{ens} = \frac{1}{2l+1} \sum_{m=-l}^{+l} \langle \overline{a_{lm}} a_{lm} \rangle_{ens} = \frac{1}{2l+1} \sum_{m=-l}^{+l} C_l = C_l$$

We can compute the variance of the estimator:

$$\begin{aligned} V(\widehat{C}_l, \widehat{C}_{l'}) &= \langle \widehat{C}_l \widehat{C}_{l'} \rangle_{ens} - \langle \widehat{C}_l \rangle \langle \widehat{C}_{l'} \rangle_{ens} \\ &= \frac{1}{(2l+1)(2l'+1)} \sum_{mm'} \langle a_{lm} \overline{a_{lm}} a_{l'm'} \overline{a_{l'm'}} \rangle_{ens} - C_l C_{l'} \end{aligned}$$

Provided that the  $a_{lm}$  are gaussian random variables, their fourth order moments can be expressed with their second order moments and we get:

$$\begin{aligned} V(\widehat{C}_l, \widehat{C}_{l'}) &= \frac{1}{(2l+1)(2l'+1)} \sum_{mm'} (C_l C_{l'} (1 + \delta_{ll'} \delta_{mm'}) + (-1)^{m+m'} C_l C_{l'} \delta_{ll'} \delta_{m-m'}) - C_l C_{l'} \\ &= \frac{1}{(2l+1)(2l'+1)} \sum_{mm'} (C_l C_{l'} + C_l^2 \delta_{ll'} \delta_{mm'}) + C_l^2 \delta_{ll'} \delta_{m-m'} - C_l C_{l'} \\ &= \frac{1}{(2l+1)(2l'+1)} \sum_{mm'} 2C_l^2 \delta_{ll'} \delta_{mm'} \\ &= \frac{2C_l^2}{2l+1} \delta_{ll'} \end{aligned}$$

Thus the  $\widehat{C}_l$  are unbiased and independent, they follow a  $\chi^2$  distribution with  $2l + 1$  degrees of freedom and their variances are:

$$\sigma_{\widehat{C}_l}^2 = \frac{2C_l^2}{2l + 1} \quad (\text{II.7})$$

Figure 1 shows an example of a power spectrum  $C_l$  and the variance of its estimator  $\widehat{C}_l$  obtain with the CMBFAST code ([Seljak et al, 1996] and [Zaldarriaga et al, 2000]) with the standard set of cosmological parameters.

### ii.3 Angular correlation function estimator.

In order to obtain an estimator  $\widehat{\xi}$  of the angular correlation function, we can average over all pairs of directions  $\vec{\Omega}, \vec{\Omega}'$  of the observed sky (keeping the angle  $\gamma$  between them fixed):

$$\widehat{\xi}(\gamma) = \frac{1}{\mathcal{N}(\gamma)} \int_{S^2 \times S^2} \overline{T}(\Omega_1) T(\Omega_2) d\Omega_1 d\Omega_2 \delta(\vec{\Omega}_1 \cdot \vec{\Omega}_2 - \cos(\gamma))$$

with

$$\mathcal{N}(\gamma) = \int_{S^2 \times S^2} d\Omega_1 d\Omega_2 \delta(\vec{\Omega}_1 \cdot \vec{\Omega}_2 - \cos(\gamma))$$

As  $T(\Omega) = \sum_{l,m} a_{lm} Y_l^m(\Omega)$ , we get:

$$\widehat{\xi}(\gamma) = \frac{1}{\mathcal{N}(\gamma)} \sum_{l_1, m_1} \sum_{l_2, m_2} \overline{a_{l_1 m_1}} a_{l_2 m_2} \int_{S^2 \times S^2} \overline{Y_{l_1}^{m_1}}(\Omega_1) Y_{l_2}^{m_2}(\Omega_2) d\Omega_1 d\Omega_2 \delta(\vec{\Omega}_1 \cdot \vec{\Omega}_2 - \cos(\gamma))$$

The internal integral  $\mathcal{I}$  is computed in appendix A and leads to the estimator value:

$$\begin{aligned} \widehat{\xi}(\gamma) &= \frac{1}{\mathcal{N}(\gamma)} \sum_{l_1, m_1} \sum_{l_2, m_2} \overline{a_{l_1 m_1}} a_{l_2 m_2} 2\pi \delta_{l_1 l_2} \delta_{m_1 m_2} P_l(\cos(\gamma)) \\ &= \frac{1}{\mathcal{N}(\gamma)} \sum_{l, m} \overline{a_{lm}} a_{lm} 2\pi P_l(\cos(\gamma)) \end{aligned}$$

Averaging over realisations gives us:

$$\begin{aligned} \langle \widehat{\xi}(\gamma) \rangle_{ens} &= \frac{1}{\mathcal{N}(\gamma)} \sum_{l, m} \langle \overline{a_{lm}} a_{lm} \rangle_{ens} 2\pi P_l(\cos(\gamma)) \\ &= \frac{1}{\mathcal{N}(\gamma)} 2\pi \sum_l (2l + 1) C_l P_l(\cos(\gamma)) \end{aligned}$$

Now  $\mathcal{N}(\gamma)$  has to be computed.  $\mathcal{N}(\gamma)$  is equal to the previously computed integral with  $T(\Omega) = 1$ . So, replacing  $T(\Omega)$  by  $\sqrt{4\pi} Y_0^0(\Omega)$ , or  $a_{lm} = \sqrt{4\pi} \delta_{l0} \delta_{m0}$  and  $C_l = 4\pi \delta_{l0}$ . As  $P_0(\cos(\gamma)) = 1$ , one finally obtains  $\mathcal{N}(\gamma) = \mathcal{N} = 8\pi^2$  and:



$$\langle \hat{\xi}(\gamma) \rangle_{ens} = \xi(\gamma) = \frac{1}{4\pi} \sum_l (2l+1) C_l P_l(\cos(\gamma)) \quad (\text{II.8})$$

The estimator  $\hat{\xi}(\gamma)$  is unbiased.

Figure 1 shows the angular correlation function  $\xi(\gamma)$  and the variance of its estimator  $\hat{\xi}(\gamma)$ .

Defining  $K = \left(\frac{2\pi}{N}\right)^2$ , the covariance of the estimator is:

$$\begin{aligned} & \frac{1}{K} \left( \langle \hat{\xi}(\gamma) \hat{\xi}(\gamma') \rangle_{ens} - \langle \hat{\xi}(\gamma) \rangle_{ens} \langle \hat{\xi}(\gamma') \rangle_{ens} \right) \\ &= \sum_{lm} \sum_{l'm'} P_l(\gamma) P_{l'}(\gamma') \langle a_{lm} \overline{a_{lm}} a_{l'm'} \overline{a_{l'm'}} \rangle_{ens} \\ & \quad - \sum_{lm} \sum_{l'm'} P_l(\gamma) P_{l'}(\gamma') \langle a_{lm} \overline{a_{lm}} \rangle_{ens} \langle a_{l'm'} \overline{a_{l'm'}} \rangle_{ens} \end{aligned}$$

As the temperature field is real, and provided that the  $a_{lm}$  are gaussian random variables, one has:

$$\begin{aligned} & \frac{1}{K} \left( \langle \hat{\xi}(\gamma) \hat{\xi}(\gamma') \rangle_{ens} - \langle \hat{\xi}(\gamma) \rangle_{ens} \langle \hat{\xi}(\gamma') \rangle_{ens} \right) \\ &= \sum_{lm} \sum_{l'm'} P_l(\gamma) P_{l'}(\gamma') C_l C_{l'} (1 + \delta_{ll'} \delta_{mm'}) + \sum_{lm} \sum_{l'm'} P_l(\gamma) P_{l'}(\gamma') C_l^2 \delta_{ll'} \delta_{m-m'} \\ & \quad - \sum_{lm} \sum_{l'm'} P_l(\gamma) P_{l'}(\gamma') C_l C_{l'} \\ &= 2 \sum_l C_l^2 P_l(\gamma) P_l(\gamma') \end{aligned}$$

Finally, by replacing  $K$  by its value, we obtain:

$$\langle \hat{\xi}(\gamma) \hat{\xi}(\gamma') \rangle_{ens} - \langle \hat{\xi}(\gamma) \rangle_{ens} \langle \hat{\xi}(\gamma') \rangle_{ens} = \frac{2}{(4\pi)^2} \sum_l (2l+1) C_l^2 P_l(\gamma) P_l(\gamma') \quad (\text{II.9})$$

The estimators of the angular correlation function values in different directions are correlated.

Figure 1 shows the correlation matrix of the angular correlation estimator  $\hat{\xi}(\gamma)$ .

#### **ii.4 What about computing the $C_l$ on a portion of sphere?**

There are two ways to compute the  $C_l$  coefficients. Given a temperature field on the sphere, one can compute the  $a_{lm}$  with (II.2) and then the  $C_l$  using the unbiased estimator (II.6). Equation (II.2) is:  $a_{lm} \sim \int P_l^m(\cos(\theta)) d\cos(\theta) \int T(\theta, \phi) e^{-im\phi} d\phi$ .

The inner integral is a Fourier transform which can be fastly computed with the Fast

Fourier Transform (FFT) technics (see [Natoli et al, 1997]). Note that this is possible only if the pixels lie on isolatitude lines. The other way is to compute the angular correlation function  $\hat{\xi}(\gamma)$ , which is unbiased, and then use the second formula in (II.5).

If the observed map is not the full sphere we can adapt these methods. For the first one we can still compute pseudo  $a_{lm}$  by setting the temperature to zero outside the observation zone. This leads to a systematic bias that will be studied in section III. This also introduces correlations among the measured  $C_l$  and increases their variances. Numerical calculations can be performed in the case where the map is a spherical cap. This is explored in section III and its last section presents detailed comparisons with simulations. This will show that the variance does not depend very much on the map shape. The evolution of the variance with the map size is interpreted in this section.

In section IV we shall discuss the use of the angular correlation function  $\hat{\xi}(\gamma)$  measured on the observed map (so the angular separation  $\gamma$  is limited to  $\gamma_{lim}$ ). We will show that this quantity is still unbiased, as one intuitively guesses. One can still use the formula (II.5) to extract the  $C_l$  but, since the correlation function is defined only on some interval  $[0, \gamma_{lim}]$ , the Legendre polynomials are no longer orthogonal. This introduces wild fluctuations in the  $C_l$ . This is cured by "apodizing" the angular correlation function and will be described in section V.

Four appendices explain technical details to make these notes self contained.

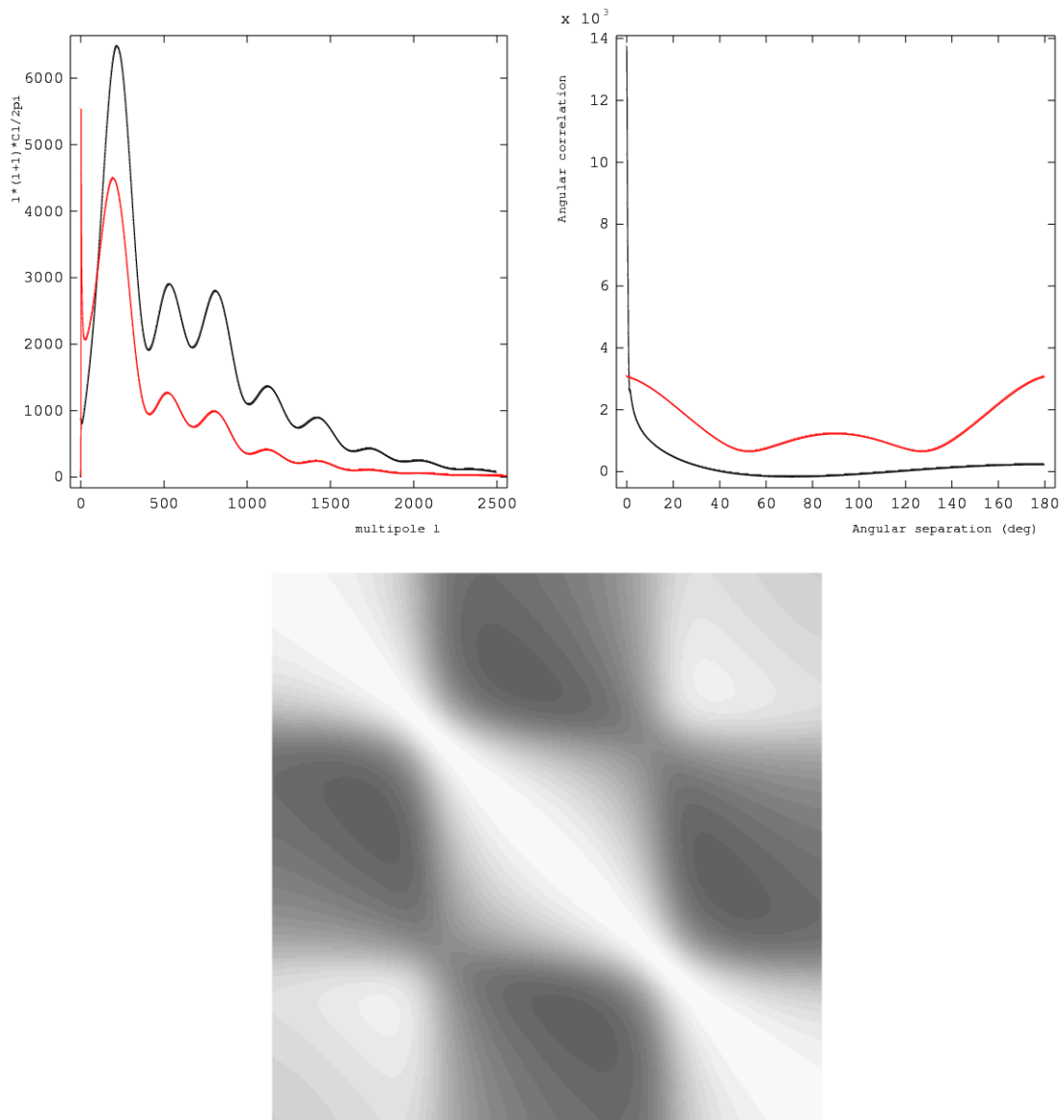


Figure 1:

► *Top left:* power spectra versus the multipole moment

► *Top right:* angular correlation function versus the separation angle (deg)

The red curves shows the dispersion of the estimator due to cosmic variance (values have been multiplied by 10 for readability)

► *Bottom:* the correlation matrix of the angular correlation function estimator.

The upper left corner is (0, 0) degree and lower right corner is (180, 180) degrees.

The LUT ranges from  $-1$  (dark) to  $1$  (white).

### III Spectrum estimation for a portion of sphere.

#### iii.1 Estimator of the $C_l$ spectrum.

The temperature field is measured on a piece  $A$  of the sphere of solid angle  $\Omega_{obs}$ . We will study the following estimator for the  $C_l$ :

$$\tilde{C}_l = \frac{1}{2l+1} \sum_{m=-l}^l |\tilde{a}_{lm}|^2 \quad (\text{III.10})$$

where the  $\tilde{a}_{lm}$  are computed on  $\Omega_{obs}$ :

$$\tilde{a}_{lm} = \int_{\Omega_{obs}} T(\Omega) \times \overline{Y_l^m}(\Omega) d\Omega \quad (\text{III.11})$$

The  $\tilde{C}_l$  will therefore represent an estimation of the spectrum of a temperature map which is set to zero outside the observed region. We define the function  $W(\vec{\Omega})$  on the sphere such that  $W = 1$  on  $A$  and 0 anywhere else.

The temperature field under study is:  $T'(\Omega) = (T \times W)(\Omega)$ .

#### iii.2 Computation of the bias of the estimator.

The function  $W$  can be expanded on spherical harmonics basis as:

$$W(\Omega) = \sum_{l=0}^{\infty} \sum_{m=-l}^l b_{lm} Y_l^m(\Omega) \quad (\text{III.12})$$

$$b_{lm} = \int_{S^2} W(\Omega) \overline{Y_l^m}(\Omega) d\Omega = \int_{\Omega_{obs}} \overline{Y_l^m}(\Omega) d\Omega \quad (\text{III.13})$$

Then the  $\tilde{a}_{lm}$  are:

$$\tilde{a}_{lm} = \int_{S^2} T(\Omega) W(\Omega) \overline{Y_l^m}(\Omega) d\Omega = \sum_{l', m', l'', m''} a_{l' m'} b_{l'' m''} \int_{S^2} Y_{l'}^{m'} Y_{l''}^{m''} \overline{Y_l^m} d\Omega$$

Using the property  $\overline{Y_l^m} = (-1)^m Y_l^{-m}$ :

$$\tilde{a}_{lm} = \sum_{l', m', l'', m''} a_{l' m'} b_{l'' m''} (-1)^m \int_{S^2} Y_{l'}^{m'} Y_l^{-m} Y_{l''}^{m''} d\Omega$$

The integral over the sphere of the product of three spherical harmonics is ([Brink et al, 1962] and [Messiah, 1964]):

$$\int_{S^2} Y_a^\alpha Y_b^\beta Y_c^\gamma \sin(\theta) d\theta d\phi = \sqrt{\frac{(2a+1)(2b+1)(2c+1)}{4\pi}} \begin{pmatrix} a & b & c \\ \alpha & \beta & \gamma \end{pmatrix} \begin{pmatrix} a & b & c \\ 0 & 0 & 0 \end{pmatrix}$$

where  $\begin{pmatrix} a & b & c \\ \alpha & \beta & \gamma \end{pmatrix}$  are the Wigner 3j symbols related to the Clebsch-Gordan coefficients by:

$$\langle aba\beta | c - \gamma \rangle = (-1)^{a-b-\gamma} \sqrt{2c+1} \begin{pmatrix} a & b & c \\ \alpha & \beta & \gamma \end{pmatrix}$$

Recall that these coefficients are real.

$$\begin{aligned} \tilde{a}_{lm} &= \sum_{l', m', l'', m''} a_{l' m'} b_{l'' m''} (-1)^m \sqrt{\frac{(2l+1)(2l'+1)(2l''+1)}{4\pi}} \begin{pmatrix} l' & l & l'' \\ m' & -m & m'' \end{pmatrix} \begin{pmatrix} l' & l & l'' \\ 0 & 0 & 0 \end{pmatrix} \\ \overline{\tilde{a}_{lm}} &= \sum_{L', M', L'', M''} \overline{a_{L' M'}} \overline{b_{L'' M''}} (-1)^m \sqrt{\frac{(2l+1)(2L'+1)(2L''+1)}{4\pi}} \begin{pmatrix} L' & l & L'' \\ M' & -m & M'' \end{pmatrix} \begin{pmatrix} L' & l & L'' \\ 0 & 0 & 0 \end{pmatrix} \end{aligned}$$

$$\begin{aligned} |\tilde{a}_{lm}|^2 &= \tilde{a}_{lm} \overline{\tilde{a}_{lm}} \\ &= \sum (a_{l' m'} \overline{a_{L' M'}}) (b_{l'' m''} \overline{b_{L'' M''}}) \times \frac{2l+1}{4\pi} \sqrt{(2l'+1)(2l''+1)(2L'+1)(2L''+1)} \\ &\quad \times \begin{pmatrix} l' & l & l'' \\ m' & -m & m'' \end{pmatrix} \begin{pmatrix} L' & l & L'' \\ M' & -m & M'' \end{pmatrix} \begin{pmatrix} l' & l & l'' \\ 0 & 0 & 0 \end{pmatrix} \begin{pmatrix} L' & l & L'' \\ 0 & 0 & 0 \end{pmatrix} \end{aligned}$$

where the sum runs on  $l', m', l'', m'', L', M', L'', M''$ .

The  $a_{lm}$  are random variables. We want to compute the average effect of finite size maps, therefore we shall perform the average over sky realisations (ensemble average<sup>2</sup>). Recalling equation (II.3), one obtains:

$$\begin{aligned} \langle \tilde{C}_l \rangle &= \frac{1}{4\pi} \sum_{m=-l}^l \sum_{l', m', l'', m'', L', M''} C_{l'} b_{l'' m''} \overline{b_{L'' M''}} (2l'+1) \sqrt{(2l''+1)(2L''+1)} \\ &\quad \times \begin{pmatrix} l' & l & l'' \\ m' & -m & m'' \end{pmatrix} \begin{pmatrix} l' & l & L'' \\ m' & -m & M'' \end{pmatrix} \begin{pmatrix} l' & l & l'' \\ 0 & 0 & 0 \end{pmatrix} \begin{pmatrix} l' & l & L'' \\ 0 & 0 & 0 \end{pmatrix} \end{aligned}$$

Now, remark that the coefficients of the Wigner 3j symbol product do not depend on  $m$  nor  $m'$ , therefore one can use the orthogonality relations

$$\sum_{\alpha\beta} \sqrt{(2c+1)(2c'+1)} \begin{pmatrix} a & b & c \\ \alpha & \beta & \gamma \end{pmatrix} \begin{pmatrix} a & b & c' \\ \alpha & \beta & \gamma' \end{pmatrix} = \delta_{cc'} \delta_{\gamma\gamma'}$$

Defining:

$$\mathcal{B}_{l''} = \frac{1}{2l''+1} \sum_{m''=-l''}^{l''} b_{l'' m''} \overline{b_{l'' m''}} \quad (\text{III.14})$$

we obtain:

$$\langle \tilde{C}_l \rangle = \frac{1}{4\pi} \sum_{l', l''} C_{l'} \mathcal{B}_{l''} (2l'+1)(2l''+1) \begin{pmatrix} l' & l & l'' \\ 0 & 0 & 0 \end{pmatrix}^2 \quad (\text{III.15})$$

<sup>2</sup> In the following, we will drop the subscript for ensemble average notations:  $\langle \dots \rangle_{ens} \rightarrow \langle \dots \rangle$

The expression of the  $3j$  symbols can be found for instance in [Brink et al, 1962]. We found recently that this calculation has already been published in [Hivon et al, 2002]. The above equation provides the relation between the true  $C_l$  and the average  $\langle \tilde{C}_l \rangle$  over many sky realisations of the  $\tilde{C}_l$  coefficients measured over a patch  $A$  of any shape of the sphere. This can be written in matrix form:

$$\left[ \langle \tilde{C}_l \rangle \right] = [M]_{ll'} \times [C_{l'}] \text{ with } M_{ll'} = \frac{2l'+1}{4\pi} \sum_{l''=0}^{\infty} (2l''+1) \mathcal{B}_{l''} \begin{pmatrix} l' & l & l'' \\ 0 & 0 & 0 \end{pmatrix}^2 \quad (\text{III.16})$$

This result is valid for any weighting function  $W$  on the sphere. The relation between the  $\tilde{C}_l$  and the  $C_l$  is linear. The matrix  $M_{ll'}$  depends only on the map shape and not on the initial  $C_{l'}$  spectrum. Permutations of 2 columns of the  $3j$  symbols change their values by a phase ([Messiah, 1964]) so  $(2l+1)M_{ll'} = (2l'+1)M_{l'l}$ . The  $M_{ll'}$  elements are positive or null.

When the full sky is observed,  $\mathcal{B}_{l''} = \mathcal{B}_0 \delta_{l''0}$  and the  $3j$  symbols imply  $l = l'$  whence  $M_{ll'}$  is the identity matrix.

On the other hand, when observing a portion of the sky, each measured  $\tilde{C}_l$  is a mixture of the  $C_l$  whose weights are given by the matrix  $M_{ll'}$ .

The properties of the matrix are illustrated in figure 4. The bottom graphs show line  $l = 1500$  of matrix  $M_{ll'}$  for a  $10 \times 10 \text{ deg}^2$  map and lines  $l = 500, 2400$  where the peaks have been shifted to  $l' = 1500$  for easy comparison: the width of the peak is nearly constant with  $l$ , that is to say that the matrix is nearly band-diagonal.

The top graphs show the  $M_{ll'}$  element values of line  $l = 1500$  for maps of various size and shapes. As the map size decreases, the peak width gets larger and a given  $\tilde{C}_l$  measurement involves a larger band in  $C_{l'}$ . The width of the peak is inversely proportionnal to the characteristic width of the map and it does not depend very much on the shape provided it is not excessively elongated. This is somewhat equivalent to what we have in Fourier analysis on small intervals.

The  $C_l$  are coefficients in the correlation function expansion (II.5). The  $P_l$  are orthogonal on  $[0, \pi]$  and form a basis on this interval. On a partial map of characteristic size  $\theta_c$  these functions are "nearly orthogonal" if they differ by more than  $\delta l \simeq \pi/\theta_c$ : loosely speaking if they have not the same number of roots in that interval. Therefore, for a given correlation function, the  $\tilde{C}_l$  will be mixtures of the "true"  $C_l$  over a range  $\simeq \delta l$ .

If  $\Omega_{obs}$  is the solid angle corresponding to the observed patch of the sky, using the completeness relation for the spherical harmonics, we have for the  $\mathcal{B}_l$  normalisation:

$$\sum_{l=0}^{\infty} (2l+1) \mathcal{B}_l = \sum_{l=0}^{\infty} \sum_{m=-l}^l b_{lm} \overline{b_{lm}} = \int_{S^2} |W(\vec{\Omega})|^2 d\vec{\Omega}$$

Until the end of this section, we assume that  $W = 1$  on  $A$  and zero elsewhere. Thus we have:

$$\sum_{l=0}^{\infty} (2l+1) \mathcal{B}_l = \Omega_{obs} \quad (\text{III.17})$$

The  $\tilde{C}_l$  are biased relative to the  $C_l$  since one observes only a fraction of the sphere, the rest being 0. Assuming that the function  $T$  is isotropic, to compare the  $\tilde{C}_l$  with  $C_l$  one

has to take into account the sky coverage normalisation:

$$\langle \tilde{C}_l^R \rangle = \frac{4\pi}{\Omega_{obs}} \times \langle \tilde{C}_l \rangle = \sum_{l'} M_{ll'}^R \times C_{l'} \quad \text{where} \quad M_{ll'}^R = \frac{4\pi}{\Omega_{obs}} M_{ll'} \quad (\text{III.18})$$

In the following, when talking about comparison between  $\tilde{C}_l$  and  $C_l$ , we will assume that the  $\tilde{C}_l$  have been renormalised as describe above.

Using the  $3j$  orthogonality relation ([Messiah, 1964], appendix C relation 15b) which gives  $\sum_{l'} (2l' + 1) \begin{pmatrix} l' & l & l'' \\ 0 & 0 & 0 \end{pmatrix}^2 = 1$  and equation (III.17) we get  $\sum_{l'} M_{ll'}^R = 1$ .

Therefore for a given  $\langle \tilde{C}_l^R \rangle$ , the sum of the weights of the  $C_{l'}$  is equal to one.

The  $\mathcal{B}_l$  can be obtain using usual computer technics (see [Gòrski et al, 2005]). Then it is easy and fast to compute numerically the matrix  $M_{ll'}$  and check the systematic effect of finite size map.

The figure 2 shows the  $\mathcal{B}_l$  spectrum and the  $M_{ll'}$  matrice for a  $10 \times 10 \text{ deg}^2$  square map.

### iii.3 Computation of the covariance of the $\tilde{C}_l$ estimator for spherical cap maps.

We have tried to compute the variance of the  $\tilde{C}_l$  estimator following the same line of calculation. Although the result does not look like too complicated, it is of little use, because it would cost a lot of computer time to be numerically calculated in the general case. However it can be calculated in the simple case of a spherical cap domain.

If, in equation (III.11), we replace the temperature field by its expression (II.1), we get:

$$\tilde{a}_{lm} = \sum_{l_1 m_1} a_{l_1 m_1} B_{l_1 m_1 lm}$$

where we have set:

$$B_{l_1 m_1 lm} = \int_{S^2} W(\vec{\Omega}) Y_{l_1}^{m_1}(\vec{\Omega}) \overline{Y_l^m(\vec{\Omega})} d\vec{\Omega}$$

Averaging over sky realisations and using equation (II.3), one gets (see details in appendix B):

$$\langle \tilde{C}_l \rangle = \frac{1}{2l+1} \sum_{m'l'm'} C_{l'} |B_{lm'l'm'}|^2 \quad \text{for} \quad -l \leq m \leq +l, \quad 0 \leq l' < \infty, \quad -l' \leq m' \leq +l'$$

and provided that the  $a_{lm}$  are *gaussian* random fields:

$$\langle \tilde{C}_l \tilde{C}_L \rangle - \langle \tilde{C}_l \rangle \langle \tilde{C}_L \rangle = \frac{2}{(2l+1)(2L+1)} \sum_{m=-l}^{+l} \sum_{M=-L}^{+L} \left| \sum_{l'} C_{l'} \sum_{m'=-l'}^{+l'} B_{l'm'l'm} \overline{B_{l'M'L'M}} \right|^2$$

The last two results are valid for any weighting function  $W$  on the sphere.  $W$  could include an additionnal weighting, for instance to treat border effects. The results of the

former section can also be adapted to that case. Until the end of this section, we will assume that  $W = 1$  on  $A$  and zero elsewhere.

This equation simplifies a lot if one considers a spherical cap centered at the north pole with border at polar angle  $\theta_c$ . Using  $Y_l^m(\theta, \phi) = \lambda_l^m(\cos(\theta)) e^{im\phi}$  (where  $\lambda_l^m$  are the normalised associated Legendre polynomials), we get in this case:

$$B_{lmLM} = 2\pi \delta_{mM} B_{lLm} \quad \text{where}^3 \quad B_{lLm} = \int_0^{\theta_c} \lambda_l^m(\cos(\theta)) \lambda_L^m(\cos(\theta)) d \cos(\theta)$$

Replacing in the general expression for the covariance, one obtains:

$$\langle \tilde{C}_l \rangle = \frac{(2\pi)^2}{2l+1} \sum_{m=-l}^l \sum_{l' \geq |m|} C_{l'} (B_{ll'm})^2 \quad (\text{III.19})$$

and for the covariance:

$$\langle \tilde{C}_l \tilde{C}_L \rangle - \langle \tilde{C}_l \rangle \langle \tilde{C}_L \rangle = \frac{2(2\pi)^4}{(2l+1)(2L+1)} \sum_m \left( \sum_{l' \geq |m|} C_{l'} B_{ll'm} B_{Ll'm} \right)^2 \quad (\text{III.20})$$

The  $B_{ll'm}$  coefficients could be computed by numerical integration but this would be very slow at high  $l$ . The calculations were done using recurrence relations.

The figure 3 shows the correlation matrix computed from the covariance formula above for a  $10 \times 10$  deg<sup>2</sup> spherical cap.

### Recurrence relations

In order to derive the following recurrence relations for the  $B_{ll'm}$  coefficients, we have used the usual recurrence relations among the normalised associated Legendre functions ([Gradshteyn et al, 1980]) which imply integrals of the form<sup>4</sup>  $\int_1^c x \lambda_l^m(x) \lambda_k^m(x) dx$ . The

latter integration can be in turn related to integrals of the type  $\int_1^c \lambda_l^m(x) \lambda_k^m(x) dx$  by

evaluating  $\int_1^c (1-x^2)(\lambda_l^{m'} \lambda_k^{m''} + \lambda_l^{m''} \lambda_k^{m'}) dx$  and using the Legendre differential equation (where ' and '' means first and second order derivations with respect to  $x$ ). One gets:

$$B_{l,l+1,m} = -c \lambda_l^m(c) \lambda_{l+1}^m(c) + \frac{\sqrt{(l+1-m)(l+1+m)}}{2(l+1)} \left( \sqrt{\frac{2l+3}{2l+1}} [\lambda_l^m(c)]^2 + \sqrt{\frac{2l+1}{2l+3}} [\lambda_{l+1}^m(c)]^2 \right)$$

<sup>3</sup> We have  $B_{ll'm} = B_{l'lm} = B_{ll'-m} \in \mathbb{R}$ ,  $B_{000} = \frac{1}{4\pi} (1 - \cos(\theta_c))$ ,  $B_{ll'm} = 0$  for  $|m| > \min(l, l')$ . From the relation  $\sum_m \overline{Y_l^m(\vec{\Omega}_1)} Y_l^m(\vec{\Omega}_2) = \frac{2l+1}{4\pi} P_l(\vec{\Omega}_1, \vec{\Omega}_2)$  we get  $\sum_m B_{llm} = \frac{2l+1}{8\pi^2} \Omega_{obs}$

<sup>4</sup> We set  $c = \cos(\theta_c)$  and  $x = \cos(\theta)$



And for  $|k - l| \geq 2$ , setting  $b = (l + 1)(k - l)(k - m)$ , one has:

$$\begin{aligned}
b \times B_{lkm} &= k \sqrt{\frac{2k+1}{2k-1}} \sqrt{\frac{2l+1}{2l+3}} \sqrt{\frac{k-m}{k+m}} \sqrt{\frac{l+1-m}{l+1+m}} (k-l-2)(l+1+m) B_{l+1,k-1,m} \\
&\quad - (k-m) \left( (l+1)c\lambda_l^m(c) - \sqrt{\frac{2l+1}{2l+3}} \sqrt{\frac{l+1+m}{l+1-m}} (l+1-m)\lambda_{l+1}^m(c) \right) \lambda_k^m(c) \\
&\quad - \sqrt{\frac{2k+1}{2k-1}} \sqrt{\frac{k-m}{k+m}} \lambda_{k-1}^m(c) \\
&\quad \times \left( k \sqrt{\frac{2l+1}{2l+3}} \sqrt{\frac{l+1-m}{l+1+m}} (l+1+m)c\lambda_{l+1}^m(c) - (k(l+1)-m^2)\lambda_l^m(c) \right)
\end{aligned} \tag{III.21}$$

This heavy recurrence relation has been verified to be numerically stable up to  $l \simeq 2500$ . The only numerical integral to perform is  $B_{llm}$ . As  $\lambda_l^m(x) \sim (1-x^2)^{\frac{1}{2}m} Q(l-m)$  (where  $Q(n)$  stands for a polynome of degree  $n$ ), the integrand of  $B_{llm}$  is a polynome of degree  $2l$  and it may be exactly computed using the Gauss-Legendre integration method with  $l+1$  points. All other  $B_{lkm}$  can be computed using the recurrence relations (III.21).

With similar technics [Wandelt et al, 2001] derived different equivalent recurrence relations.

### Approximation for small maps

For small  $\theta_c$  ( $\theta_c \lesssim 0.15$ ), one can make the approximation ([Gradshtein et al, 1980]):

$$\lambda_l^m(\cos(\theta)) \rightarrow \frac{(-1)^m}{l^m} \sqrt{\frac{(2l+1)(l+m)!}{4\pi(l-m)!}} J_m(l\theta)$$

where the  $J_m$  are the cylindrical Bessel functions. Therefore:

$$B_{l_1lm} \simeq \sqrt{\frac{2l+1}{4\pi} \frac{2l_1+1}{4\pi} \frac{(l+m)! (l_1+m)!}{(l-m)! (l_1-m)!}} \frac{1}{l_1^m l^m} \int_0^{\theta_c} \theta J_m(l_1\theta) J_m(l\theta) d\theta$$

where the last integral is a Lommel integral ([Gradshtein et al, 1980]). Then:

$$\begin{aligned}
B_{l_1lm} &\simeq \sqrt{\frac{2l+1}{4\pi} \frac{2l_1+1}{4\pi} \frac{(l+m)! (l_1+m)!}{(l-m)! (l_1-m)!}} \frac{1}{l_1^m l^m} \frac{\theta_c}{l_1^2 - l^2} \\
&\quad \times \{l J_m(l_1\theta_c) J'_m(l\theta_c) - l_1 J_m(l\theta_c) J'_m(l_1\theta_c)\}
\end{aligned} \tag{III.22}$$

where  $J'_m(z)$  stands for the derivative of  $J_m(z)$  relative to  $z$ .

For numerical purposes it is easier to replace  $\{l J_m(l_1\theta_c) J'_m(l\theta_c) - l_1 J_m(l\theta_c) J'_m(l_1\theta_c)\}$  by  $\{l_1 J_m(l\theta_c) J_{m+1}(l_1\theta_c) - l J_m(l_1\theta_c) J_{m+1}(l\theta_c)\}$ . Figure 9 compares the variance of the  $\tilde{C}_l^R$  computed with relation (III.21) with the calculation done with the above approximation: the agreement is excellent for  $f_{sky} = \frac{\Omega_{obs}}{4\pi} \lesssim 6 \cdot 10^{-3}$  ( $\theta_c \lesssim 0.15$  rd).

### Behaviour of the variance as a function of $\theta_c$

If  $l\theta_c < m$ ,  $J_m(l\theta_c)$  behaves as  $(l\theta_c)^m$  which gives a negligible contribution if  $m$  is large. On the other hand, if  $m < l\theta_c$  one can use the following approximation ([Gradshtein et al, 1980]):

$$J_m(l\theta_c) \simeq \sqrt{\frac{2}{\pi}} \frac{1}{\sqrt{l\theta_c}} \cos(l\theta_c + \phi_m)$$

where  $\phi_m$  is a phase depending on  $m$  and slowly varying with  $l\theta_c$ :  $\phi_m \rightarrow -m\frac{\pi}{2} - \frac{\pi}{4}$  for  $l\theta_c \rightarrow \infty$ .

In that approximation, from equation (III.22) one obtains<sup>5</sup>:

$$B_{l_1 l m} \sim \frac{\sin((l_1 - l)\theta'_c)}{l_1 - l} \quad \theta'_c = \theta_c + \text{corrections depending on } m \quad (\text{III.23})$$

One can use this approximation in equation (III.20) in which we set  $l = L$  for the variance calculation.

If only the central peak of  $B_{l_1 m}^2$  as a function of  $l_1$  is considered ( $|l_1 - l| \lesssim \pi/\theta_c$ ) the partial sum  $\sum_l$  in equation (III.20) behaves as  $\theta_c$  because  $B_{l_1 m}^2$  is a function with a peak height proportionnal to  $\theta_c^2$  and width  $\pi/\theta_c$ . A more systematic calculation shows that, due to the high values of  $C_l$  at low  $l$ , one can not neglect the contribution of  $B_{l_1 m}^2$  at the left of the peak ( $l_1 < l - \pi/\theta_c$ ).

The sum over  $m$  in equation (III.20) introduces a factor  $\sim 2l\theta_c$ .

If one considers only the central peak (and using the normalisation in formula (III.18)), one gets  $\sigma_{\tilde{C}_l^R}^2 \sim \frac{\sigma_{C_l}^2(4\pi)}{\theta_c}$ , so  $\sigma_{\tilde{C}_l^R}$  would scale as  $f_{sky}^{-\frac{1}{4}}$ .

Numerically we found that a good approximation for small  $\theta_c$  is:

$$\sigma_{\tilde{C}_l^R} \sim \frac{\sigma_{C_l}(4\pi)}{\sqrt{f_{sky}} \sqrt{\frac{\pi}{\theta_c}}} \quad (\text{III.24})$$

For large  $l$  values, the peak wing corrections lead to corrections of higher order in  $1/\theta_c$ :

$$\sigma_{\tilde{C}_l^R}^2 \sim \frac{\sigma_{C_l}^2(4\pi)}{\theta_c} \times (1 + \frac{b(l)}{\theta_c} + \dots) \quad (\text{III.25})$$

### ***iii.4 Discussion and comparison with simulations***

In the following the  $\tilde{C}_l$  coefficients are computed from simulated CMB maps using the well known Fast Fourier Transform (FFT) technics ([Natoli et al, 1997]).

Simulations have been realised using the HEALPIX package ([Gòrski et al, 2005]). Pure CMB maps of various sizes and shapes have been simulated using the program SYNFAST with  $l_{max} = 2500$  for the standard  $\Lambda$ CDM spectrum. The temperature field outside the various observed regions is set to zero.

The pixel size was chosen small enough ( $NSIDE = 2048$ ) in order not to bias the  $C_l$  reconstruction up to  $l_{max} = 2500$ . The pixel smoothing windows has been chosen to be that of a  $NSIDE = 8192$ . So the value in a pixel is very nearly the value of the temperature field at the center of the pixel. No detector noise nor telescope lobe effect was added.

The  $C_l$  were reconstructed using the program ANAFast up to  $l_{max} = 2500$ . That is to say that ANAFast computes our  $\tilde{C}_l$  as defined in equation (III.10).

Using full sphere simulations we checked that the reconstructed  $\hat{C}_l$  were in perfect agreement, even at large  $l$ , with the generated ones. Table (1) shows the generations used in the following discussion. In the following  $f_{sky} = \frac{\Omega_{obs}}{4\pi}$  is the fraction of the observed sky.

<sup>5</sup> This equation and (III.19) explain qualitatively the behaviour of the matrix  $M_{ll'}$ .

map size	$f_{sky}$	number of generations
$4\pi sr$	1	579
$20 \times 32$	$1.54 \cdot 10^{-2}$	228
$17 \times 17$	$0.697 \cdot 10^{-2}$	579
$R = 9.585$	-	2279
$10 \times 10$	$0.242 \cdot 10^{-2}$	228
$6 \times 6$	$0.872 \cdot 10^{-3}$	228
$4 \times 9$	-	228
$R = 3.385$	-	228

Table 1: Description of simulations:  $R = \theta_c$  means a spherical cap with polar angle  $\theta_c$  deg, other maps are labeled  $\Delta\theta \times \Delta\phi$  deg<sup>2</sup>.

Figure 5 shows that the bias computed using formulae (III.16) and (III.18) is in excellent agreement with the simulations. Figure 6 illustrates the fact, with  $17 \times 17$  deg<sup>2</sup> maps, that this systematic bias may not be small with respect to the variance. In the present figure it is of the order of  $2\sigma$  for  $l \geq 2000$ . We note also that the correction can be important at lower  $l$  although dominated by the variance. The  $\tilde{C}_l^R$  values are systematically above the input  $C_l$  when  $200 \lesssim l$  and are oscillating with a period  $\delta l \simeq \pi/\theta_c$ . The matrix  $M_{ll'}$  (III.16) has long oscillating quasi-symmetric tails (see the figure 4). The input  $C_l$  spectrum used is a rapidly decreasing function. Therefore the left tail contribution is much larger than the right tail one, making the bias always positive at high  $l$ . The observed oscillations are a consequence of the  $M_{ll'}$  matrix oscillating tails and of the global shape of the  $C_l$  spectrum, but are not, at first order, the image of the acoustic peaks. A smooth input  $C_l$  spectrum without peaks leads also to an oscillating  $\tilde{C}_l^R$  spectrum with only a slightly different pattern. For a more rapidly decreasing input spectrum, the amplitude of the oscillations increases.

The variance has been computed numerically using (III.20) and the recurrence relations (III.21). The results are compared with various simulations in figures 7 and 8. They show that the variance can be predicted accurately independently of the map shape, although the calculations were performed for spherical caps. The figure 8 shows in detail the agreement between spherical cap map simulations and calculations. We can even go further and compare the correlation matrix obtained from simulations to the calculations for spherical caps:

$$Cor(l, L) = \frac{\langle \tilde{C}_l \tilde{C}_L \rangle - \langle \tilde{C}_l \rangle \langle \tilde{C}_L \rangle}{\sqrt{\langle \tilde{C}_l^2 \rangle - \langle \tilde{C}_l \rangle^2} \sqrt{\langle \tilde{C}_L^2 \rangle - \langle \tilde{C}_L \rangle^2}}$$

We will do the comparison for a few lines of the correlation matrix. Figure 10 compares computation and simulation for two lines ( $l = 2001$  and  $l = 1500$ ) of the correlation matrix around the correlation peak for  $f_{sky} = 0.697 \cdot 10^{-2}$  (see table (1)). Top plots are for a spherical cap (2279 simulations) and bottom ones are for a square map (579 simulations). When  $l, L$  are both larges, the dispersion is rather small. The top left plot shows the very good agreement between computation and simulations. The bottom left plot shows that, even for a square map, the correlation peak is well reproduced. Outside the peak, the correlation level is fairly good but out of phase due to the map shape. The same conclusions can be drawn for the right plots although dispersion in the simulations

is larger because of the large variance we have for small values of  $l, L$ . In conclusion, the correlation peak shape is rather independent of the map shape. We note also that the correlation matrix outside the diagonal region has a periodic structure of period  $\simeq 2\pi/\theta_c$  which is a consequence of formula (III.23).

Figure 11 shows  $\sigma_{\tilde{C}_l^R}/\sigma_{C_l}(4\pi)$  versus  $f_{sky}$  for various  $l$ . The variance ( $\sigma_{\tilde{C}_l^R}^2$ ) does not scale as  $f_{sky}^{-1}$  as often assumed (see the discussion in ([Tegmark, 1997])). The black dashed curve shows  $\sigma_{\tilde{C}_l^R}/\sigma_{C_l}(4\pi) = \frac{1}{\sqrt{f_{sky}}}$ .

For  $l \sim 500$  the variance scale as  $f_{sky}^{-\frac{1}{2}}$  as expected from the lowest order calculation (formula (III.24)) represented by the solid black curve. For larger  $l$  values, we have to take into account the correction terms of formula (III.25). This indicates that the dependance of the variance on the map size depends also on the  $C_l$  spectrum shape.

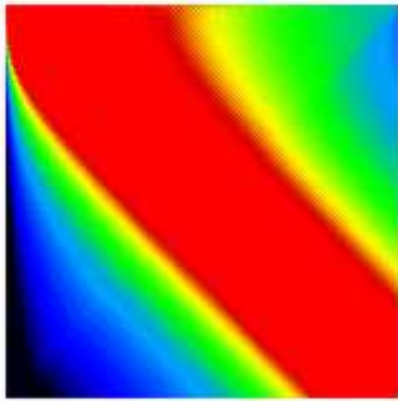
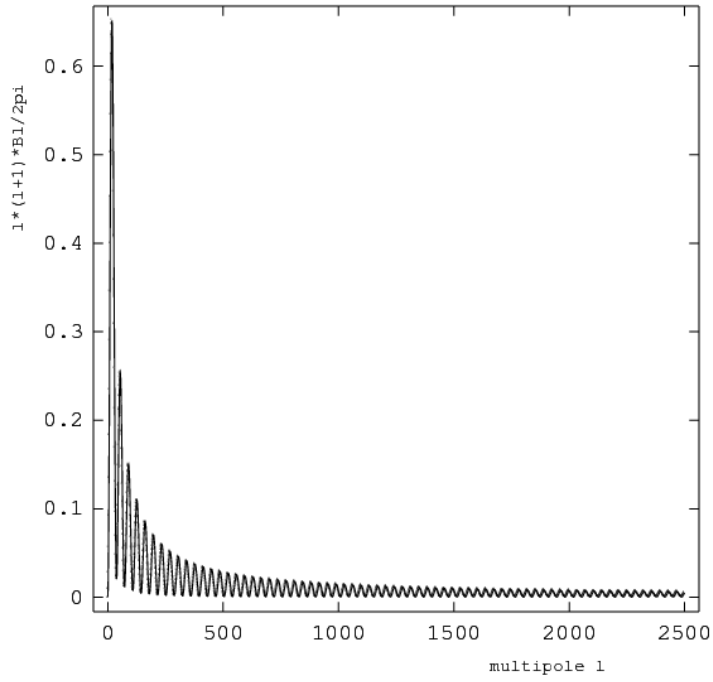


Figure 2: The top picture shows the  $\mathcal{B}_l$  spectrum for a  $10 \times 10 \text{ deg}^2$  square map. The bottom picture shows the matrix  $M_{ll'}$  for the same map (The LUT as been optimised for readability purpose). Axes range from upper corner left ( $l = 0, l' = 0$ ) to bottom right corner ( $l = 2500, l' = 2500$ ).

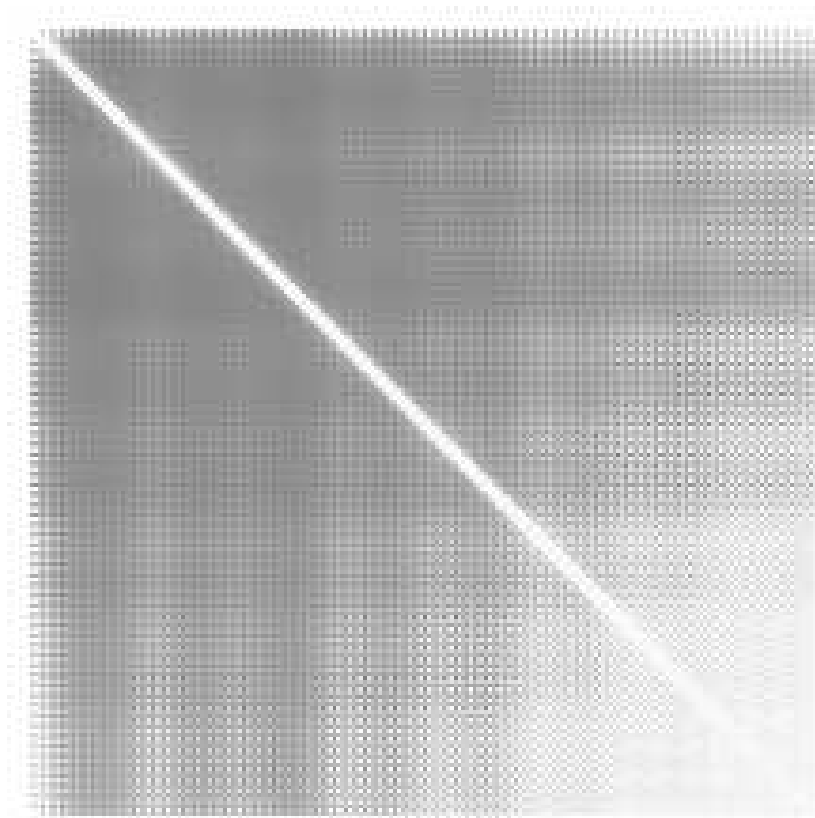


Figure 3: Correlation matrix for the  $\tilde{C}_l$  a  $10 \times 10 \text{ deg}^2$  spherical cap. The top left corner is for  $(l = 0, l' = 0)$  and the bottom left corner is for  $(l = 2500, l' = 2500)$ . The LUT ranges from  $-1$  (dark) to  $+1$  (white).

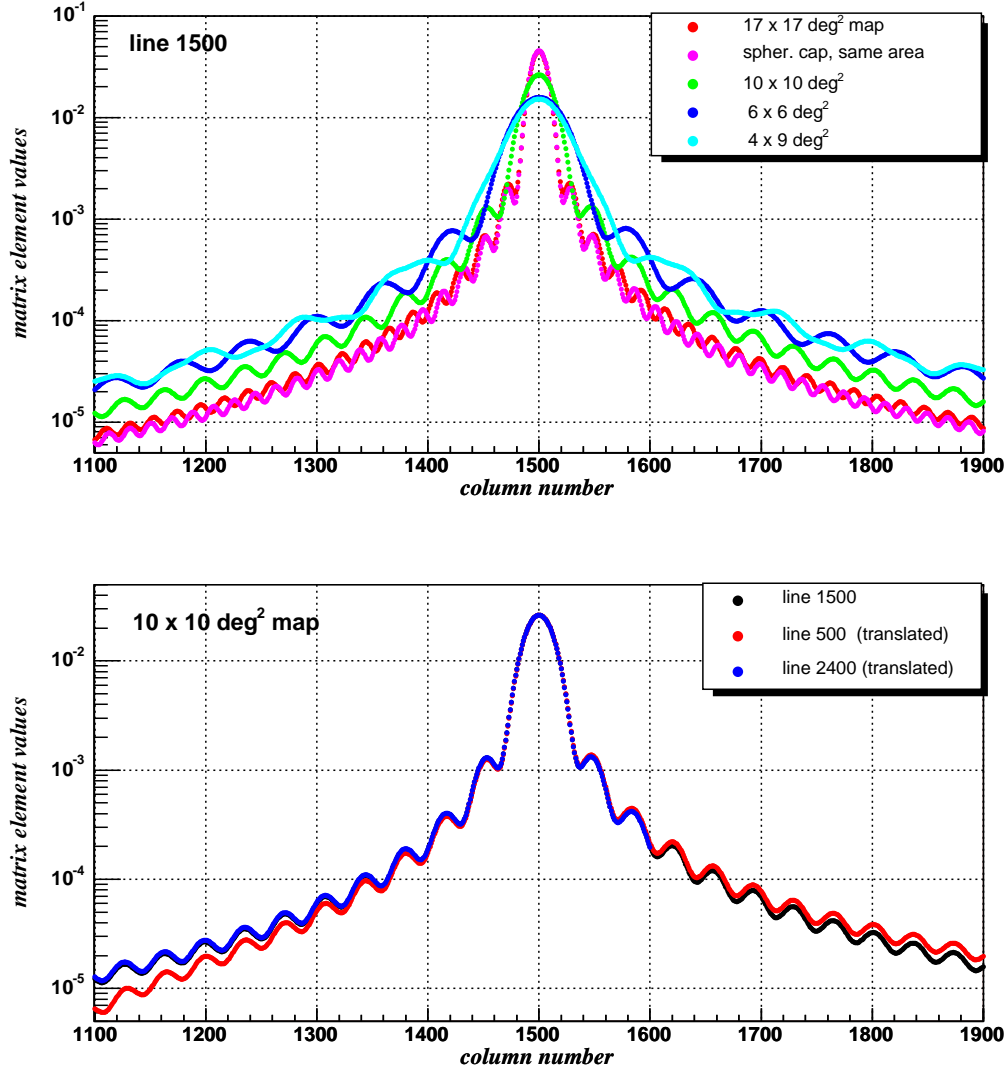


Figure 4: The top picture shows line  $l = 1500$  of matrix  $M_{ll'}$  for  $l'$  ranging from 1100 to 1900 and for maps of various sizes and shapes. The bottom one shows line  $l = 1500$  of matrix  $M_{ll'}$  for a  $10 \times 10 \text{ deg}^2$  map and lines  $l = 500, 2400$  where the peaks have been shifted to  $l' = 1500$  for easy comparison.

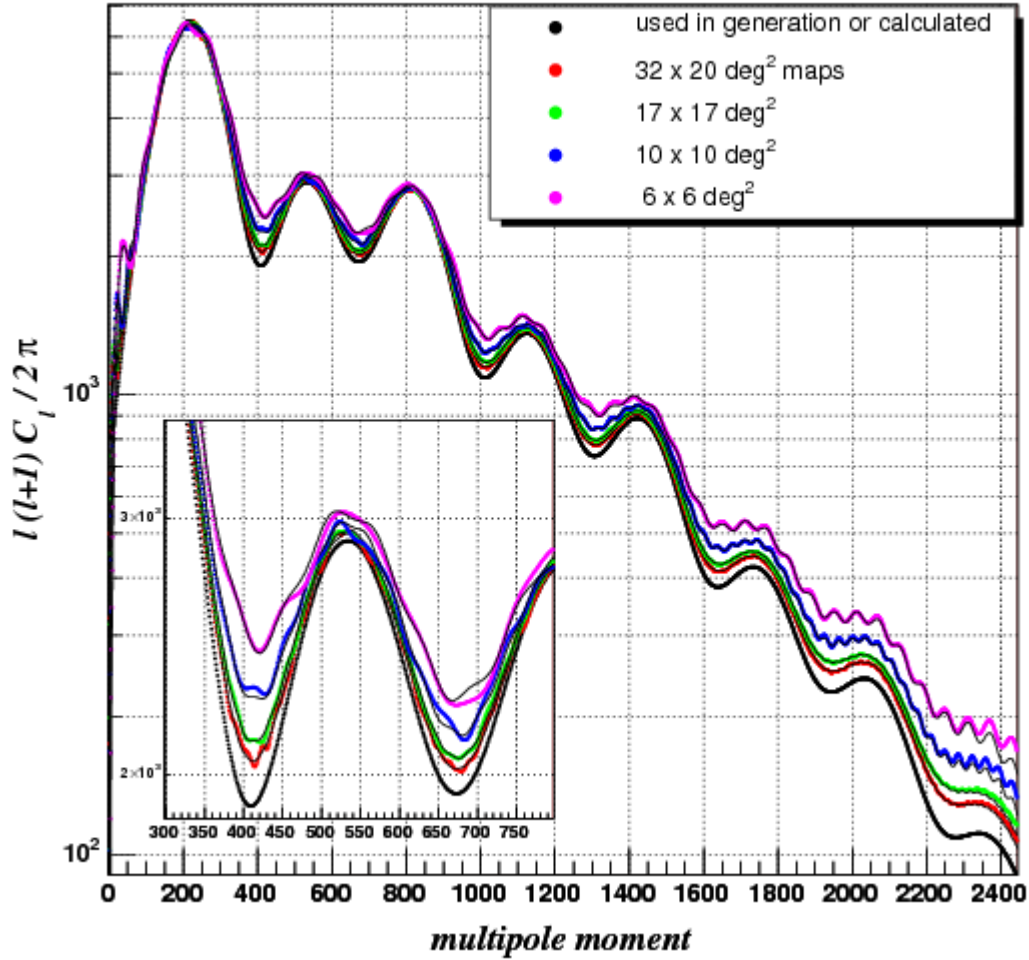


Figure 5: Systematic effect on  $C_l$  for various size maps. The thick black curve represents the  $C_l$  coefficients used in the simulations. The colored curves show the average  $\langle \tilde{C}_l^R \rangle$  reconstructed from simulations for various map sizes. The thin black curves superimposed on colored ones show the results predicted by formula (III.16).



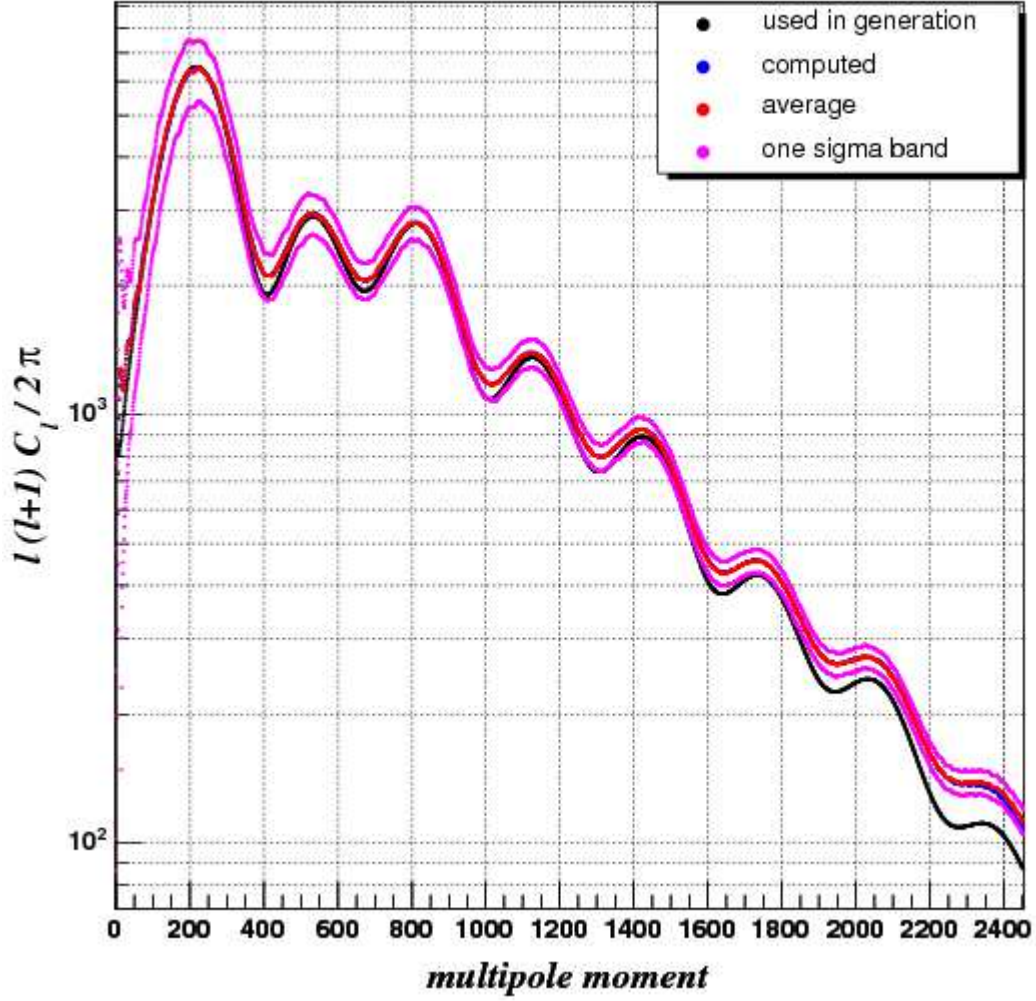


Figure 6: Finite size map systematic effect on  $C_l$  for a  $17 \times 17 \text{ deg}^2$  map. The thick black curve represents the  $C_l$  used in the simulations. The red curve show the average  $\langle \tilde{C}_l^R \rangle$  reconstructed from simulations. The two pink curves show the one sigma deviation reconstructed from simulations. The blue curve shows the results predicted by formula (III.16).

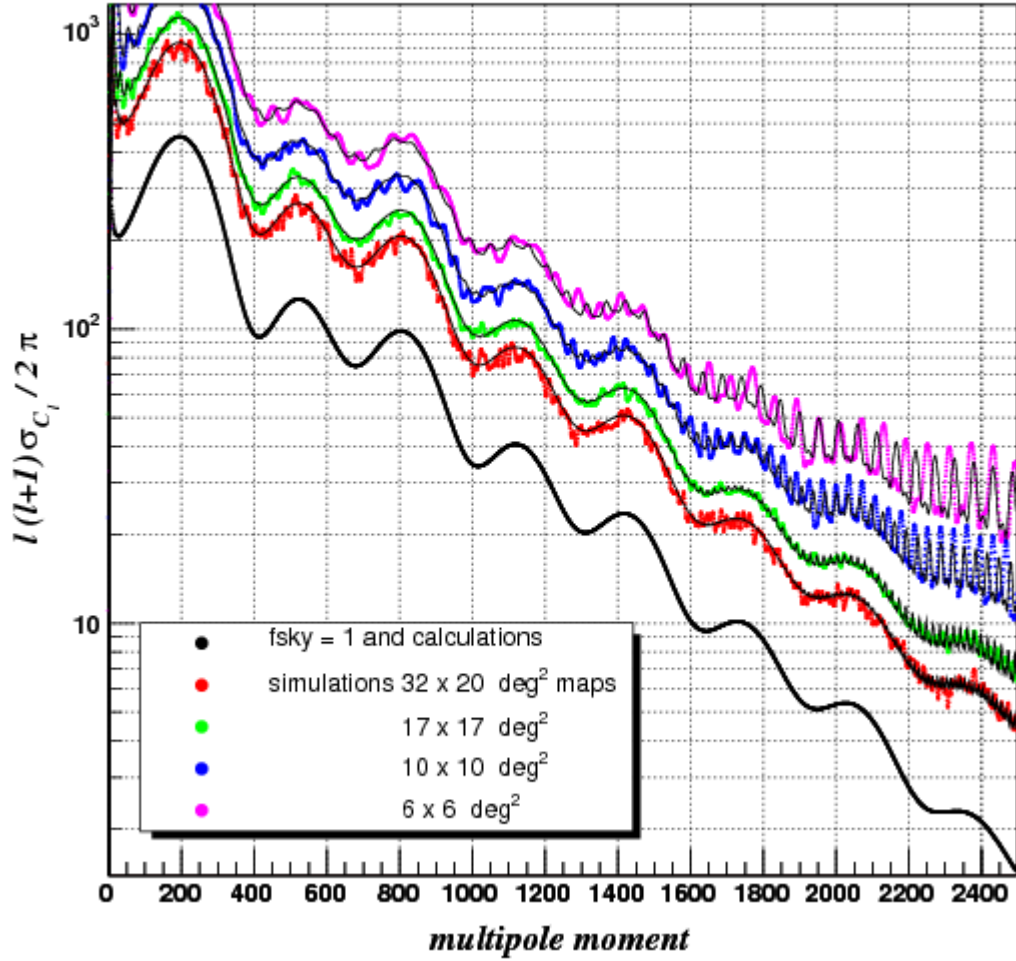


Figure 7: Finite size map effect on  $C_l$  variance for various maps. The thick black curve represents the variance of the  $\widehat{C}_l$  for the full sphere. The colored curves show the variance of the  $\widetilde{C}_l^R$  reconstructed from simulations. The thin black curves superimposed on colored ones show the results predicted by formula (III.21).

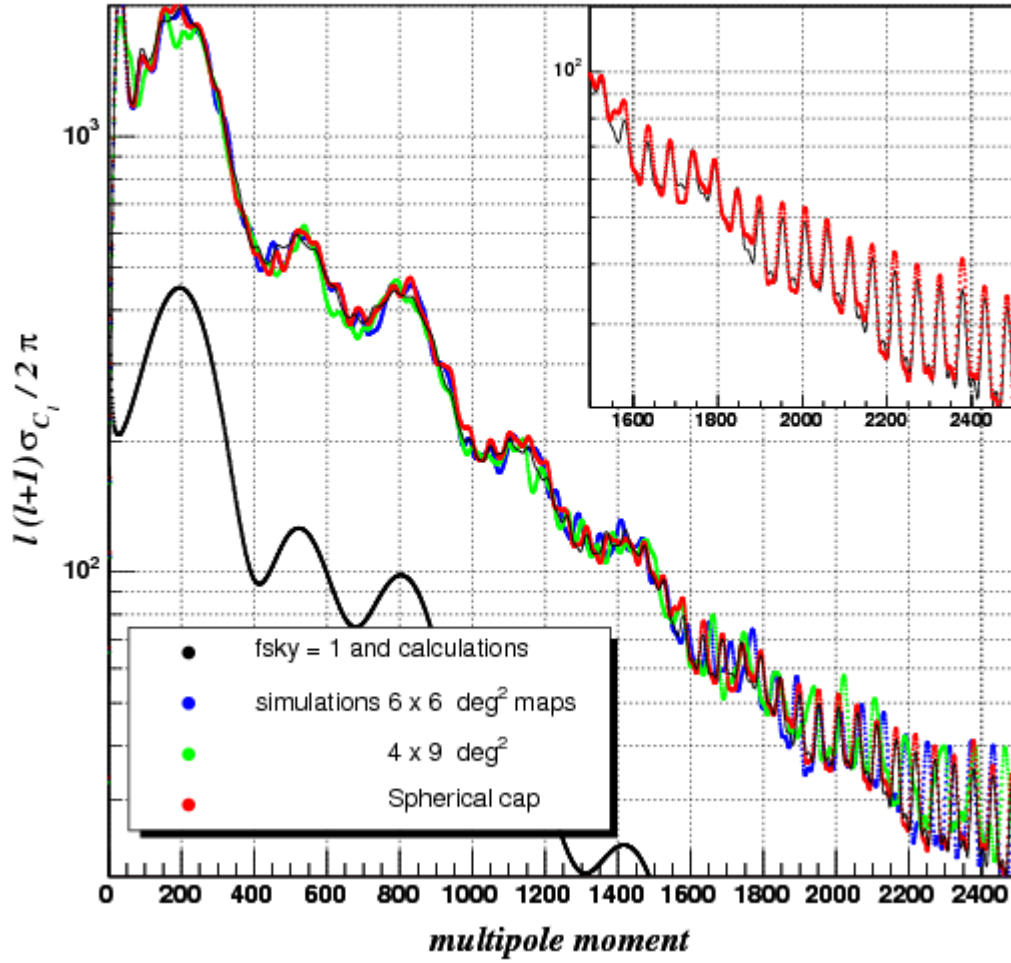


Figure 8: Finite size map effect on  $C_l$  variance for various  $\sim 36 \text{ deg}^2$  maps with different shapes. The zoom compares the result of simulations for spherical cap with the formula (III.21).

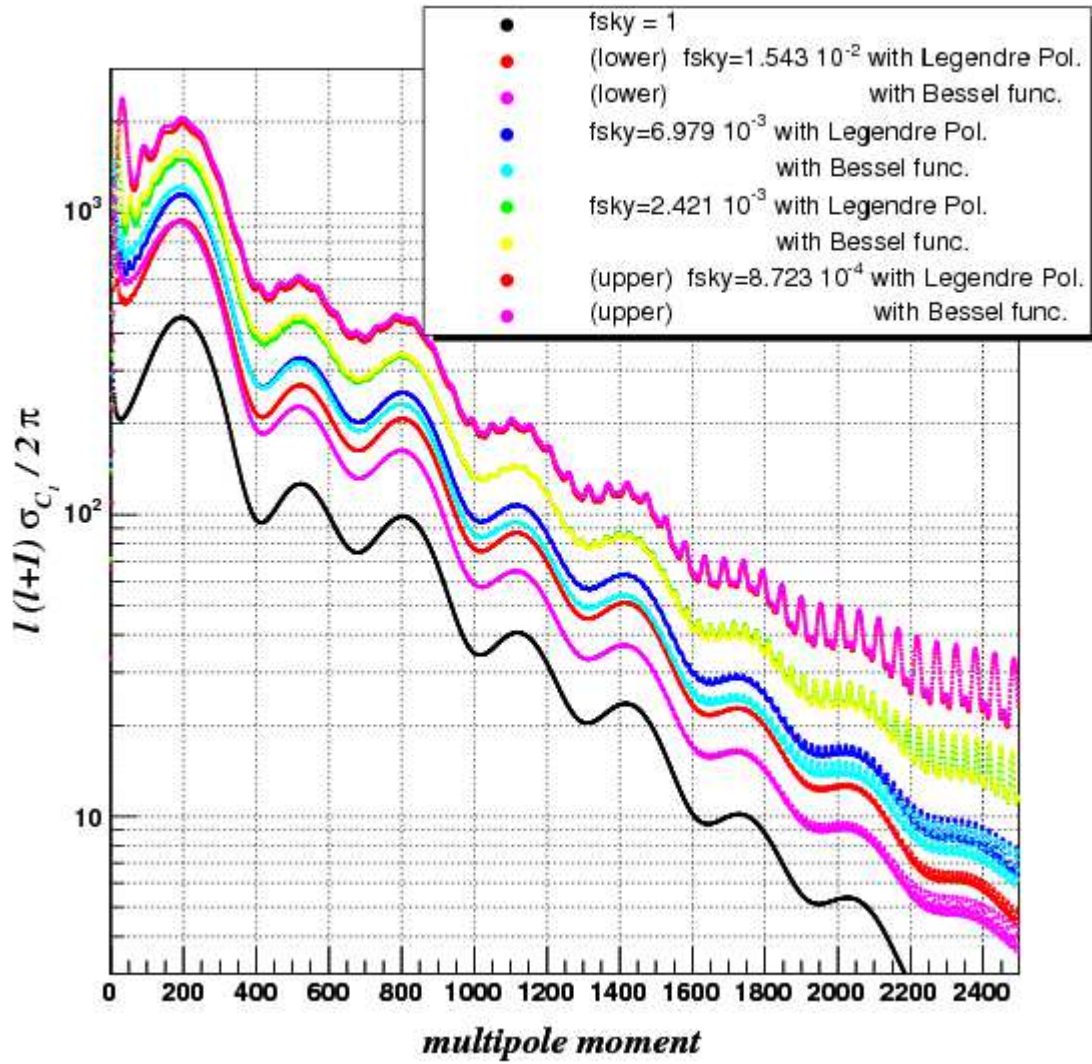


Figure 9: Validity of the small polar cap map approximation. Comparison of the variance computed with Legendre polynomials and Bessel function approximations (see section (iii.3)).

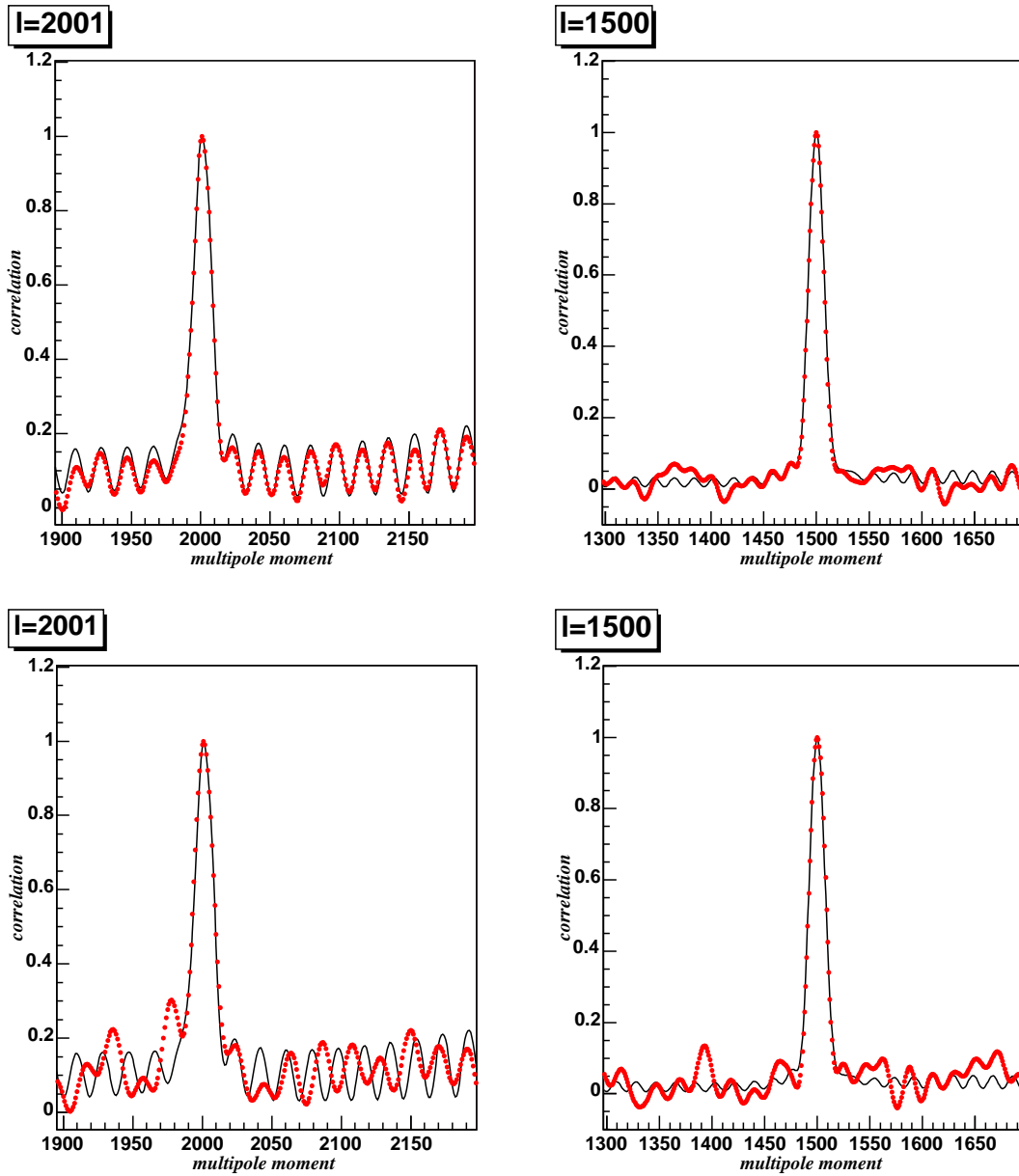


Figure 10: Comparison of the computed correlation matrix with simulations for  $17 \times 17 \text{ deg}^2$  maps. Black curves correspond to the computed correlation for a spherical cap. Red curves represent the correlation computed from simulations: the top figures correspond to a spherical cap and the bottom figures to a square map. The lines  $l = 2001$  and  $l = 1500$  of the correlation matrix  $Cor(l, L)$  are drawn versus columns  $L$  around the correlation peak.

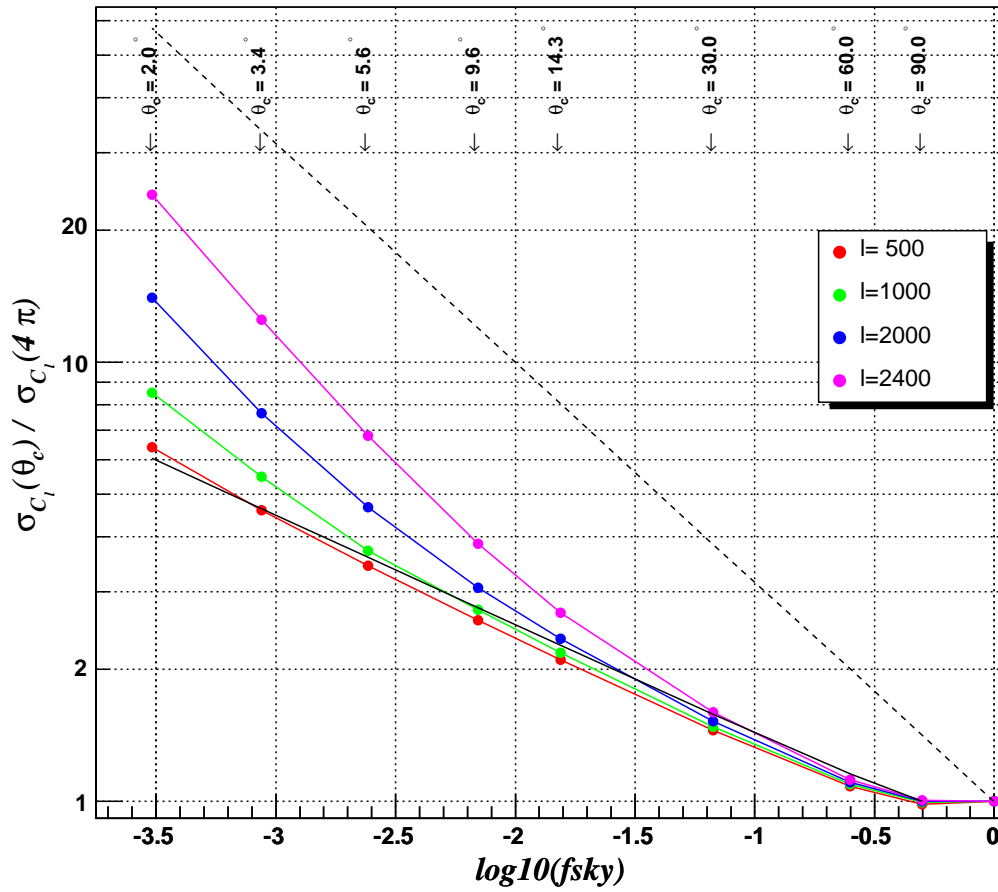


Figure 11: Square root of the variance of  $C_l$  relative to the full sphere variance versus map aperture  $\theta_c$  for various  $l$ . The black dashed curve represents the simple  $f_{sky}^{-\frac{1}{2}}$  scaling. The black solid curve represents the first order scaling (equation (III.24)).

## IV Angular correlation function estimation for a portion of sphere.

### iv.1 Estimator of the angular correlation function.

The angular correlation function  $\tilde{\xi}(\gamma)$  is estimated as in section ii.3 but with the integration limited to the portion of sphere  $A$ . Let's define :

$$W^A(\Omega) = 1 \text{ if } \Omega \in A \text{ and } 0 \text{ elsewhere, or } W(\Omega) > 0 \text{ in } A \text{ and } 0 \text{ elsewhere.}$$

The angular correlation function can be computed without ponderation on the temperature field. We define:

$$\begin{aligned} \tilde{\xi}(\gamma) &= \frac{1}{\mathcal{N}^A(\gamma)} \int_{A \times A} d\Omega_1 d\Omega_2 \overline{T(\Omega_1)} T(\Omega_2) \delta(\vec{\Omega}_1 \cdot \vec{\Omega}_2 - \cos(\gamma)) \\ &= \frac{1}{\mathcal{N}^A(\gamma)} \int_{S^2 \times S^2} d\Omega_1 d\Omega_2 \overline{T(\Omega_1)} \overline{W^A(\Omega_1)} T(\Omega_2) W^A(\Omega_2) \delta(\vec{\Omega}_1 \cdot \vec{\Omega}_2 - \cos(\gamma)) \end{aligned}$$

or more generally with a ponderation  $W(\Omega)$ :

$$\begin{aligned} \tilde{\xi}(\gamma) &= \frac{1}{\mathcal{N}^A(\gamma)} \int_{A \times A} d\Omega_1 d\Omega_2 \overline{T(\Omega_1)} \overline{W(\Omega_1)} T(\Omega_2) W(\Omega_2) \delta(\vec{\Omega}_1 \cdot \vec{\Omega}_2 - \cos(\gamma)) \\ &= \frac{1}{\mathcal{N}^A(\gamma)} \int_{S^2 \times S^2} d\Omega_1 d\Omega_2 \overline{T(\Omega_1)} \overline{W(\Omega_1)} T(\Omega_2) W(\Omega_2) \delta(\vec{\Omega}_1 \cdot \vec{\Omega}_2 - \cos(\gamma)) \end{aligned}$$

with

$$\begin{aligned} \mathcal{N}^A(\gamma) &= \int_{A \times A} d\Omega_1 d\Omega_2 \delta(\vec{\Omega}_1 \cdot \vec{\Omega}_2 - \cos(\gamma)) \\ &= \int_{S^2 \times S^2} d\Omega_1 d\Omega_2 \overline{W^A(\Omega_1)} W^A(\Omega_2) \delta(\vec{\Omega}_1 \cdot \vec{\Omega}_2 - \cos(\gamma)) \end{aligned}$$

We have  $T(\Omega) = \sum_{LM} a_{lm} Y_l^m(\Omega)$  and we define:

$$\begin{cases} W(\Omega) = \sum_{LM} b_{LM} Y_L^M(\Omega) \\ W^A(\Omega) = \sum_{LM} b_{LM}^A Y_L^M(\Omega) \end{cases}$$

The above integral becomes:

$$\begin{aligned} \mathcal{N}^A(\gamma) \tilde{\xi}(\gamma) &= \sum_{\dots} \overline{a_{l_1 m_1}} \overline{b_{L_1 M_1}} a_{l_2 m_2} b_{L_2 M_2} \\ &\quad \times \int_{S^2 \times S^2} d\Omega_1 d\Omega_2 \delta(\vec{\Omega}_1 \cdot \vec{\Omega}_2 - \cos(\gamma)) \overline{Y_{l_1}^{m_1}}(\Omega_1) \overline{Y_{L_1}^{M_1}}(\Omega_1) Y_{l_2}^{m_2}(\Omega_2) Y_{L_2}^{M_2}(\Omega_2) \end{aligned}$$

where the sum  $\sum$  goes over  $\{l_1, m_1, L_1, M_1, l_2, m_2, L_2, M_2\}$ .

The computation is described in details in appendix C. We get:

$$\langle \tilde{\xi}(\gamma) \rangle = \left( \sum_l \frac{2l+1}{4\pi} C_l P_l(\gamma) \right) \frac{\sum_L (2L+1) \mathcal{B}_L P_L(\gamma)}{\sum_L (2L+1) \mathcal{B}_L^A P_L(\gamma)}$$

where  $\mathcal{B}_l$  and  $\mathcal{B}_l^A$  are defined respectively with  $b_{lm}$  and  $b_{lm}^A$  according to (III.14), and

$$\mathcal{N}^{(A)}(\gamma) = 2\pi \sum_L (2L+1) \mathcal{B}_L^{(A)} P_L(\gamma)$$

For  $\gamma > \Theta_{max}$ , where  $\Theta_{max}$  is the largest angular distance on the map  $A$ ,  $\tilde{\xi}(\gamma)$  is not computable.

• If  $W = W^A$ , the temperature field is not ponderated on  $A$  and the estimator is unbiased:

$$\langle \tilde{\xi}(\gamma) \rangle = \sum_l \frac{2l+1}{4\pi} C_l P_l(\gamma) = \xi(\gamma)$$

• If  $W \neq W^A$ , the temperature field is ponderated on  $A$  by the positive function  $W(\Omega)$  and the angular correlation function is biased.

• If the temperature field is ponderated on  $A$  by the positive function  $W(\Omega)$  and we replace  $\mathcal{N}^A(\gamma)$  by:

$$\mathcal{N}^W(\gamma) = \int_{S^2 \times S^2} d\Omega_1 d\Omega_2 \overline{W(\Omega_1)} W(\Omega_2) \delta(\vec{\Omega}_1 \cdot \vec{\Omega}_2 - \cos(\gamma)) = 2\pi \sum_L (2L+1) \mathcal{B}_L P_L(\gamma)$$

the estimator is unbiased.

Note that  $\mathcal{N}^A(\gamma)$  is proportional to the number of pairs of directions separated by an angle  $\gamma$  that can be done on  $A$ .

## iv.2 Comparison of the estimator with the $\langle \tilde{C}_l \rangle$ .

$\langle \tilde{\xi}(\gamma) \rangle$  can also be expressed relative to the ensemble average  $\langle \tilde{C}_l \rangle$  of the bias  $C_l$  computed in section iii.2.

We have ( $c = \cos(\gamma)$ ):

$$\mathcal{N}^A(c) \tilde{\xi}(c) = \sum_{lm'l'm'} \overline{a_{lm}} a_{l'm'} \int_{A \times A} d\Omega d\Omega' \delta(\vec{\Omega} \cdot \vec{\Omega}' - c) \overline{Y_l^m(\Omega)} Y_{l'}^{m'}(\Omega')$$

The integral is computed in appendix D. Computing the ensemble average gives:

$$\begin{aligned} \mathcal{N}^A(c) \langle \tilde{\xi}(c) \rangle &= \sum_{lm'l'm'LM} C_l \delta_{ll'} \delta_{mm'} \times (2\pi P_L(c) B_{LMlm} \overline{B_{LMl'm'}}) \\ &= 2\pi \sum_{lmLM} C_l P_L(c) |B_{LMlm}|^2 \\ &= 2\pi \sum_L P_L(c) \sum_{lmM} C_l |B_{LMlm}|^2 \\ &= 2\pi \sum_L P_L(c) (2L+1) \langle \tilde{C}_L \rangle \end{aligned}$$

We finally obtain:

$$\langle \tilde{\xi}(\gamma) \rangle = 2\pi \sum_l (2l+1) \frac{P_l(\gamma)}{\mathcal{N}^A(\gamma)} \langle \tilde{C}_l \rangle$$



### iv.3 Covariance of the estimator of the angular correlation function on partial map.

Let's define  $c_1 = \cos(\gamma_1)$  and  $c_2 = \cos(\gamma_2)$ .

$$\mathcal{N}^A(c_1) \tilde{\xi}(c_1) = \sum_{\dots} \overline{a_{l_1 m_1}} a_{l'_1 m'_1} \int_{A \times A} d\Omega_1 d\Omega'_1 \delta(\vec{\Omega}_1 \cdot \vec{\Omega}'_1 - c_1) \overline{Y_{l_1}^{m_1}}(\Omega_1) Y_{l'_1}^{m'_1}(\Omega'_1)$$

where the sum  $\sum$  goes over  $\{l_1, m_1, l'_1, m'_1\}$ .

$$\begin{aligned} \mathcal{N}^A(c_1) \mathcal{N}^A(c_2) &< \tilde{\xi}(c_1) \tilde{\xi}(c_2) > \\ &= < a_{l'_1 m'_1} \overline{a_{l_1 m_1}} a_{l'_2 m'_2} \overline{a_{l_2 m_2}} > \int_{A \times A} d\Omega_1 d\Omega'_1 \delta(\vec{\Omega}_1 \cdot \vec{\Omega}'_1 - c_1) \\ &\quad \times \int_{A \times A} d\Omega_2 d\Omega'_2 \delta(\vec{\Omega}_2 \cdot \vec{\Omega}'_2 - c_2) \overline{Y_{l_1}^{m_1}}(\Omega_1) Y_{l'_1}^{m'_1}(\Omega'_1) \overline{Y_{l_2}^{m_2}}(\Omega_2) Y_{l'_2}^{m'_2}(\Omega'_2) \end{aligned}$$

If the temperature field is real and gaussian, we can compute the fourth moment of the  $a_{lm}$ . That leads to 3 terms:

$$\begin{aligned} 1 - / & C_{l'_1} C_{l'_2} \dots Y_{l'_1}^{m'_1}(\Omega'_1) \overline{Y_{l'_1}^{m'_1}}(\Omega_1) Y_{l'_2}^{m'_2}(\Omega'_2) \overline{Y_{l'_2}^{m'_2}}(\Omega_2) \\ 2 - / & C_{l'_1} C_{l'_2} \dots Y_{l'_1}^{m'_1}(\Omega'_1) Y_{l'_2}^{m'_2}(\Omega_1) Y_{l'_2}^{m'_2}(\Omega'_2) \overline{Y_{l'_1}^{m'_1}}(\Omega_2) \\ 3 - / & (-1)^{m'_1+m_1} C_{l'_1} C_{l_1} \dots Y_{l'_1}^{m'_1}(\Omega'_1) \overline{Y_{l_1}^{m_1}}(\Omega_1) Y_{l'_1}^{-m'_1}(\Omega_2) \overline{Y_{l_1}^{-m_1}}(\Omega_2) \end{aligned}$$

The first term gives  $< \mathcal{N}^A(c_1) \tilde{\xi}(c_1) > < \mathcal{N}^A(c_2) \tilde{\xi}(c_2) >$ . Using  $Y_l^m = (-1)^m \overline{Y_l^{-m}}$  and playing with indices, it is easy to demonstrate that the second and third terms are equal. We have:

$$\begin{aligned} \mathcal{N}^A(c_1) \mathcal{N}^A(c_2) &\left( < \tilde{\xi}(c_1) \tilde{\xi}(c_2) > - < \tilde{\xi}(c_1) > < \tilde{\xi}(c_2) > \right) \\ &= \mathcal{N}^A(c_1) \mathcal{N}^A(c_2) V(\tilde{\xi}(c_1), \tilde{\xi}(c_2)) \\ &= 2 \times \sum_{l_1 m_1 l'_1 m'_1} C_{l'_1} C_{l_1} \\ &\quad \times \int_{A \times A} d\Omega_1 d\Omega'_1 \delta(\vec{\Omega}_1 \cdot \vec{\Omega}'_1 - c_1) Y_{l'_1}^{m'_1}(\Omega'_1) \overline{Y_{l_1}^{m_1}}(\Omega_1) \\ &\quad \times \int_{A \times A} d\Omega_2 d\Omega'_2 \delta(\vec{\Omega}_2 \cdot \vec{\Omega}'_2 - c_2) Y_{l_1}^{m_1}(\Omega_2) \overline{Y_{l'_1}^{m'_1}}(\Omega'_2) \\ &= 2 \times \sum_{l_1 m_1 l'_1 m'_1} C_{l'_1} C_{l_1} I_{l'_1 m'_1}^{l_1 m_1}(c_1) I_{l_1 m_1}^{l'_1 m'_1}(c_2) \end{aligned}$$

where:

$$I_{l'_1 m'_1}^{l_1 m_1}(c) = \int_{A \times A} d\Omega d\Omega' \delta(\vec{\Omega} \cdot \vec{\Omega}' - c) Y_{l'_1}^{m'_1}(\Omega') \overline{Y_{l_1}^{m_1}}(\Omega) = \overline{I_{l_1 m_1}^{l'_1 m'_1}(c)}$$

is computed in appendix D. Going back to the computation of the  $\tilde{\xi}(c)$  covariance:

$$\begin{aligned}
& \mathcal{N}^A(c_1)\mathcal{N}^A(c_2) V(\tilde{\xi}(c_1), \tilde{\xi}(c_2)) \\
&= 2(2\pi)^2 \sum_{l_1 m_1 l'_1 m'_1} C_{l_1} C_{l'_1} I_{l_1 m_1}^{l_1 m_1}(c_1) I_{l'_1 m'_1}^{l'_1 m'_1}(c_2) \\
&= 2(2\pi)^2 \sum_{l_1 m_1 l'_1 m'_1} \sum_{LML'M'} C_{l_1} C_{l'_1} P_L(c_1) P_{L'}(c_2) B_{LMl_1 m_1} \overline{B_{LMl'_1 m'_1}} B_{L'M'l'_1 m'_1} \overline{B_{L'M'l_1 m_1}} \\
&= 2(2\pi)^2 \sum_{LML'M'} P_L(c_1) P_{L'}(c_2) \left( \sum_{l_1 m_1} C_{l_1} B_{LMl_1 m_1} \overline{B_{L'M'l_1 m_1}} \right) \left( \sum_{l'_1 m'_1} C_{l'_1} B_{L'M'l'_1 m'_1} \overline{B_{LMl'_1 m'_1}} \right) \\
&= 2(2\pi)^2 \sum_{LML'M'} P_L(c_1) P_{L'}(c_2) \left| \sum_{lm} C_l B_{L'M'lm} \overline{B_{LMlm}} \right|^2 \\
&= 2(2\pi)^2 \sum_{LL'} P_L(c_1) P_{L'}(c_2) \left( \sum_{MM'} \left| \sum_{lm} C_l B_{L'M'lm} \overline{B_{LMlm}} \right|^2 \right)
\end{aligned}$$

The term in parenthesis can be expressed relative to the covariance  $V_{\tilde{C}_i}(L, L')$  of the  $\tilde{C}_i$  (see appendix B):

$$\begin{aligned}
\mathcal{N}^A(c_1)\mathcal{N}^A(c_2) V(\tilde{\xi}(c_1), \tilde{\xi}(c_2)) &= 2(2\pi)^2 \sum_{LL'} P_L(c_1) P_{L'}(c_2) \left( \frac{(2L+1)(2L'+1)}{2} V_{\tilde{C}_i}(L, L') \right) \\
&= (2\pi)^2 \sum_{LL'} (2L+1)(2L'+1) V_{\tilde{C}_i}(L, L') P_L(c_1) P_{L'}(c_2)
\end{aligned}$$

Using the value of  $\mathcal{N}^A(\gamma)$  computed in section C, one finally obtain for a partial map of any shape:

$$\begin{aligned}
V(\tilde{\xi}(c_1), \tilde{\xi}(c_2)) &= \langle \tilde{\xi}(c_1) \tilde{\xi}(c_2) \rangle - \langle \tilde{\xi}(c_1) \rangle \langle \tilde{\xi}(c_2) \rangle \\
&= \frac{(2\pi)^2 \sum_{l,l'} (2l+1)(2l'+1) V_{\tilde{C}_i}(l, l') P_l(\gamma_1) P_{l'}(\gamma_2)}{\mathcal{N}^A(\gamma_1) \mathcal{N}^A(\gamma_2)} \\
&= \frac{\sum_{l,l'} (2l+1)(2l'+1) V_{\tilde{C}_i}(l, l') P_l(\gamma_1) P_{l'}(\gamma_2)}{\left( \sum_L (2L+1) \mathcal{B}_L^A P_L(\gamma_1) \right) \left( \sum_{L'} (2L'+1) \mathcal{B}_{L'}^A P_{L'}(\gamma_2) \right)}
\end{aligned}$$

Recall that the  $V_{\tilde{C}_i}(l, l')$  can only be computed easily if the partial map is a spherical cap. The figure 12 shows the correlation matrix of the  $\tilde{\xi}(\gamma)$  for a spherical cap of area  $17 \times 17 \text{ deg}^2$ : one sees that the level of correlation is very high.



Figure 12: Correlation matrix of the  $\tilde{\xi}(\gamma)$  for a  $17 \times 17 \text{ deg}^2$  spherical cap. The top left corner is for  $(\gamma = 0, \gamma' = 0)$  and the bottom left corner is for  $(\gamma = 19.1, \gamma' = 19.1 \text{ deg})$ . The LUT ranges from 0.5 (dark) to +1 (white).

## V $C_l$ estimation using the angular correlation function

### for a portion of sphere.

#### v.1 Using integration of the angular correlation function.

Suppose that we measure the angular correlation function  $\tilde{\xi}(\gamma)$ .  
For the full sphere we have:

$$C_l = 2\pi \int_{\gamma=0}^{\pi} \xi(\gamma) P_l(\cos(\gamma)) d \cos(\gamma)$$

On a portion of sphere, we may have an estimation of the  $C_l$  by performing the integration

$$\tilde{C}_l^\xi = 2\pi \int_{\gamma=0}^{\theta_{lim}} \tilde{\xi}(\gamma) P_l(\cos(\gamma)) d \cos(\gamma) \quad (\text{V.26})$$

where  $\theta_{lim}$  is the maximum separation angle obtainable for that map.  
We demonstrated that  $\tilde{\xi}(\gamma)$  is unbiased, so:

$$\langle \tilde{\xi}(\gamma) \rangle = \xi(\gamma) = \frac{1}{4\pi} \sum_{l=0}^{\infty} (2l+1) C_l P_l(\cos(\gamma))$$

Thus we compute:

$$\begin{aligned} \langle \tilde{C}_l^\xi \rangle &= 2\pi \int_{\gamma=0}^{\theta_{lim}} \langle \tilde{\xi}(\gamma) \rangle P_l(\cos(\gamma)) d \cos(\gamma) \\ &= 2\pi \int_{\gamma=0}^{\theta_{lim}} \xi(\gamma) P_l(\cos(\gamma)) d \cos(\gamma) \\ &= 2\pi \frac{1}{4\pi} \sum_{l'=0}^{\infty} (2l'+1) C_{l'} \int_{\gamma=0}^{\theta_{lim}} P_{l'}(\cos(\gamma)) P_l(\cos(\gamma)) d \cos(\gamma) \end{aligned}$$

Using the definition of the  $B_{Llm}$ , the  $P_l$  and the  $\lambda_l^0$  we have:

$$\langle \tilde{C}_l^\xi \rangle = 2\pi \sum_{l'=0}^{\infty} \sqrt{\frac{2l'+1}{2l+1}} C_{l'} B_{l'l0}$$

with  $B_{l'l0} \equiv B_{l'l0}(\theta_{lim})$ .

► As we have a sharp cut-off at  $\theta_{lim}$ , the obtained spectrum oscillates strongly around the theoretical value (that is somewhat equivalent to the Gibbs phenomena we have with the Fourier transform), and that method is not usable. The figure 13 shows the predicted  $\tilde{C}_l^\xi$  for a spherical cap of angular aperture  $\theta_{lim} = 19 \text{ deg}$ . The level of oscillations is very high. The “wave length” of the oscillations is about  $\Delta l \sim \frac{2\pi}{\theta_{lim}}$ . This problem is discussed in the next section.

One can compute the covariance of the  $\tilde{C}_l^\xi$ :

$$\langle \tilde{C}_l^\xi \tilde{C}_{l'}^\xi \rangle = (2\pi)^2 \int_0^{\theta_{lim}} \langle \tilde{\xi}(\gamma) \tilde{\xi}(\gamma') \rangle P_l(\cos(\gamma)) P_{l'} \tilde{\xi}(\cos(\gamma')) d \cos(\gamma) d \cos(\gamma')$$

Using the variance of the  $\tilde{\xi}$  computed in section iv.3, we obtain:

$$V(\tilde{C}_l^\xi, \tilde{C}_{l'}^\xi) = \sum_{l_1 l'_1} M_{ll_1} V_{\tilde{C}_l}(l_1, l'_1) M_{l'l'_1} \quad (\text{V.27})$$

with

$$M_{ll_1} = (2\pi)^2 (2l_1 + 1) \int_0^{\theta_{lim}} \frac{1}{\mathcal{N}^A(\gamma)} P_l(\gamma) P_{l_1}(\gamma) d \cos(\gamma) \quad (\text{V.28})$$

## *v.2 Using integration of a smooth apodization of the angular correlation function.*

In order to avoid the problem shown in figure 13 due to the sharp cut-off at  $\theta_{lim}$ , the correlation function  $\tilde{\xi}(\gamma)$  is multiplied by a function going smoothly to zero at  $\theta_{lim}$ .

A usefull function is:  $F_{tanh}(\theta) = \frac{1}{2}(1 - \tanh(\frac{\theta - \theta_0}{\Delta}))$  where  $\theta_0$  is the cutting angle and  $\Delta$  characterises the width of the smoothing.

One could also take  $F_{erf}(\theta) = \frac{1}{2}(1 - erf(\frac{\theta - \theta_0}{\Delta}))$ .

The estimator in (V.26) is changed to:

$$\tilde{C}_l^\xi = 2\pi \int_{\gamma=0}^{\theta_{lim}} \tilde{\xi}(\gamma) F(\gamma) P_l(\cos(\gamma)) d \cos(\gamma) \quad (\text{V.29})$$

In that case the average value of the estimator is:

$$\begin{aligned} \langle \tilde{C}_l^\xi \rangle &= 2\pi \int_{\gamma=0}^{\theta_{lim}} \langle \tilde{\xi}(\gamma) \rangle F(\gamma) P_l(\cos(\gamma)) d \cos(\gamma) \\ &= \frac{1}{2} \sum_{l'=0}^{\infty} (2l' + 1) C_{l'} \int_{\gamma=0}^{\theta_{lim}} P_{l'}(\cos(\gamma)) P_l(\cos(\gamma)) F(\gamma) d \cos(\gamma) \end{aligned}$$

It has to be computed numerically.

The covariance keeps the same form as (V.27) if we replace  $M_{ll_1}$  in the former section by:

$$M_{ll_1} = (2\pi)^2 (2l_1 + 1) \int_0^{\theta_{lim}} \frac{1}{\mathcal{N}^A(\gamma)} P_l(\gamma) P_{l_1}(\gamma) F(\gamma) d \cos(\gamma) \quad (\text{V.30})$$

### ► Apodization effect for small maps.

We compute:  $I = \int_{\theta=0}^{\theta_{lim}} P_{l'}(\cos(\theta)) P_l(\cos(\theta)) F(\theta) d\cos(\theta)$ . For  $\theta_{lim}$  small, we may approximate  $P_l(\cos(\theta)) \simeq J_0(l\theta)$  and we have ( $\sin(\theta) \simeq \theta$ ):

$$I = \int_0^{\theta_{lim}} J_0(l'\theta) J_0(l\theta) F(\theta) \theta d\theta$$

We define:  $L(\theta) = \int_0^{\theta} J_0(l'\theta') J_0(l\theta') \theta' d\theta'$  which is a Lommel integral. Integrating  $I$  by parts:

$$I = [L(\theta) F(\theta)]_0^{\theta_{lim}} - \int_0^{\theta_{lim}} L(\theta) \frac{d}{d\theta} F(\theta) d\theta$$

But  $L(0) = 0$  and we set the smoothing function to be null at  $\theta_{lim}$  i.e.  $F(\theta_{lim}) = 0$ . Thus  $[\dots]_0^{\theta_{lim}} = 0$  and we have:

$$I = - \int_0^{\theta_{lim}} L(\theta) \frac{d}{d\theta} F(\theta) d\theta$$

To perform analytical computations, we take:  $F(\theta) = F_{erf}(\theta) = \frac{1}{2}(1 - erf(\frac{\theta-\theta_0}{\Delta}))$ , we have:  $\frac{d}{d\theta} F_{erf} = -\frac{1}{\sqrt{\pi}\Delta} \exp\left(-\frac{(\theta-\theta_0)^2}{\Delta^2}\right)$  and we obtain:

$$I = \frac{1}{\sqrt{\pi}\Delta} \int_0^{\theta_{lim}} L(\theta) \exp\left(-\frac{(\theta-\theta_0)^2}{\Delta^2}\right) d\theta$$

The Lommel integral  $L(\theta)$  is ([Gradshteyn et al, 1980]):

$$L(\theta) = \frac{\theta}{l'^2 - l^2} [lJ_0(l'\theta)J_0'(l\theta) - l'J_0(l\theta)J_0'(l'\theta)]$$

where  $J_0'(x)$  is the derivative with respect to  $x$ , and we make the approximation (for  $l\theta_{lim} \gg 1$ ):  $J_0(l\theta) \simeq \sqrt{\frac{2}{\pi l\theta}} \cos(l\theta + \phi)$  with  $\phi \rightarrow -(n + \frac{1}{2})\frac{\pi}{2}$  if  $\theta \rightarrow \infty$ . For  $J_0$ , this remains a good approximation even for values as low as  $l\theta \simeq 4$ .

We obtain:  $L(\theta) = \frac{1}{\pi} \frac{1}{\sqrt{l'l'}} \left[ \frac{\sin((l'-l)\theta)}{l'-l} + \frac{\sin((l'+l)\theta+2\phi)}{l'+l} \right]$

The second term is of order  $\frac{1}{l'+l}$  with respect to the first one and will be neglected. We finally have:

$$\begin{aligned} I &\propto \frac{1}{\Delta\sqrt{l'l'}} \int_0^{\theta_{lim}} \frac{\sin((l'-l)\theta)}{l'-l} \exp\left(-\frac{(\theta-\theta_0)^2}{\Delta^2}\right) d\theta \\ &\propto \frac{1}{\Delta\sqrt{l'l'}} \int_{-\infty}^{+\infty} \frac{\sin((l'-l)\theta)}{l'-l} \exp\left(-\frac{(\theta-\theta_0)^2}{\Delta^2}\right) d\theta \end{aligned}$$

where we have replaced the integration limits because  $\Delta \ll \theta_0$  so that the integrand is null outside the limits. Setting  $z = \theta - \theta_0$  we have:

$$\sin((l'-l)\theta) = \sin((l'-l)(\theta_0 + z)) = \sin((l'-l)\theta_0) \cos((l'-l)z) + \cos((l'-l)\theta_0) \sin((l'-l)z)$$

Thus:

$$I \propto \frac{1}{\Delta\sqrt{l'}} \left\{ \frac{\sin((l'-l)\theta_0)}{l'-l} \int_{-\infty}^{+\infty} \cos((l'-l)z) \exp(-\frac{z^2}{\Delta^2}) dz + \cos((l'-l)\theta_0) \int_{-\infty}^{+\infty} \frac{\sin((l'-l)z)}{l'-l} \exp(-\frac{z^2}{\Delta^2}) dz \right\}$$

The second integral is null by symmetry:

$$I \propto \frac{\theta_0}{\Delta\sqrt{l'}} \frac{\sin((l'-l)\theta_0)}{(l'-l)\theta_0} \int_{-\infty}^{+\infty} \cos((l'-l)z) \exp(-\frac{z^2}{\Delta^2}) dz$$

As  $\int_{-\infty}^{\infty} \cos((l'-l)x) \exp(-x^2/\Delta^2) dx = \sqrt{\pi} \Delta \exp(-\frac{1}{4}(l'-l)^2\Delta^2)$ , we have:

$$I \propto \frac{\theta_0}{\sqrt{l'}} \frac{\sin((l'-l)\theta_0)}{(l'-l)\theta_0} \exp(-\frac{1}{4}(l'-l)^2\Delta^2)$$

and finally:

$$\langle \tilde{C}_l^\xi \rangle \propto \sum_{l'=0}^{\infty} (2l'+1) C_{l'} \frac{\theta_0}{\sqrt{l'}} \frac{\sin((l'-l)\theta_0)}{(l'-l)\theta_0} \exp(-\frac{1}{4}(l'-l)^2\Delta^2)$$

The value of a  $\langle \tilde{C}_l^\xi \rangle$  is given by a kind of convolution:

- The width of the *sinc* goes like  $\frac{1}{\theta_0}$ , so as  $\theta_0$  goes to zero, the width will become large.
- The width of the gaussian goes like  $\frac{1}{\Delta}$  ( $\sigma = \frac{\sqrt{2}}{\Delta}$ ), so the larger the width of the smoothing function (large  $\Delta$ ), the smaller the width of the gaussian in the last formula.

The oscillations described in the previous section (see figure 13) are due to the contribution of the low multipoles at high  $l$ : if there is no apodization, as there is a lot of power in low  $l$  multipoles, the high  $l$  multipoles will get a lot of power transferred from the low ones and the oscillations will be large:

- If the apodization is too sharp, the width of the gaussian will be very large and the “convolution” will be dominated by the *sinc*. The “sinc” decrease slowly ( $1/l$ ), the transfert of power from the low multipole to the high ones will be important and so will be the oscillations. We need a smooth apodization function.
- If  $\theta_0$  is large the width of the *sinc* will be small and the oscillation of the *sinc* will remain imprinted on the spectrum. We must take  $\theta_0$  not near  $\theta_{lim}$ .

The figure 14 shows the effect of various apodization parameters on the predicted  $C_l$  (formula V.29). The apodizations are applied to the “theoretical angular correlation function” with  $\theta_{lim} \sim 19 \text{ deg}$  corresponding to  $17 \times 17 \text{ deg}^2$  spherical cap maps.

- for  $\theta_0 = 15 \text{ deg}$ ,  $\Delta = 0.5 \text{ deg}$ : the spectrum oscillates at low  $l$  due to the sharpness of the filter. At high  $l$  it is undistinguishable from the theoretical one.

- for  $\theta_0 = 10 \text{ deg}, \Delta = 5 \text{ deg}$ : the angular correlation spectrum is not apodized enough near  $\theta_{lim}$  and, as explained above, the low multipoles  $C_l$  values correlate with the high multipole ones leading to oscillations at high  $l$  in the reconstructed spectrum.
- $\theta_0 = 1 \text{ deg}, \Delta = 2 \text{ deg}$  shows that one cannot lower too much  $\theta_0$  without losing information. The reconstructed spectrum becomes highly biased and smoothed.
- $\theta_0 = 10 \text{ deg}, \Delta = 2 \text{ deg}$  shows an example of good apodization. The reconstructed spectrum differs only at very low multipole values where the size of the map becomes too small.

Using V.27 with V.30, the top plot of figure 15 shows the variance  $l(l+1)\sigma_{\tilde{C}_l^\xi}/2\pi$  for ( $\theta_0 = 10 \text{ deg}, \Delta = 2 \text{ deg}$ ) and ( $\theta_0 = 10 \text{ deg}, \Delta = 5 \text{ deg}$ ): because of the poor apodization of the second filter, the variance increases a lot at high multipoles.

The bottom plot of figure 15 shows the correlation function for  $l = 1500$  for ( $\theta_0 = 10 \text{ deg}, \Delta = 2 \text{ deg}$ ) and ( $\theta_0 = 5 \text{ deg}, \Delta = 2 \text{ deg}$ ): the width of the correlation peak depends on the value of  $\theta_0$  and is greater for the second filter as the accessible separation angle in the angular correlation spectrum is lower in that case.

### *v.3 Practical $C_l$ reconstruction from the angular correlation spectrum.*

The above analytical results were applied to a set of 173 simulated  $17 \times 17 \text{ deg}^2$  square maps to check the quality of the  $C_l$  reconstruction. Computing the correlation spectrum is time consuming, therefore, for practical purposes, the temperature field has been calculated on a rectangular grid with constant  $\theta$  and  $\phi$  intervals of  $1 \text{ arcmin}$ , across the equator. The temperature field is obtained using SYNFAST (see [Gòrski et al, 2005]) with  $NSIDE = 4096$  and attributing to the grid nodes the temperature value of the nearest HEALPIX map cell center. No telescope lobe nor measurement noise was introduced. The separation angle is computed only from the  $\theta$  and  $\phi$  differences which allows fast computation of the angular correlation histogram. We have checked that, for the small maps under consideration, this procedure does not introduce any bias by simulating maps with the same area but largely elongated along the equator. Reconstructed angular correlation spectra are shown in figure 16 as functions of  $\gamma$ , not  $\cos(\gamma)$ , because the high angular momentum information is at small values of  $\gamma$ . The spectra are very different, one from the other, due to the large low  $l$  value variance of the  $C_l$ .

Reconstructing the  $C_l$  spectrum from these correlation histograms requires some care. First, at high  $l$  values, the Legendre polynomials oscillate rapidly and the calculation of the integral (V.29) must be performed with a very small angular step. For that purpose, the correlation spectrum histograms have been oversampled by a factor 10 and the intermediate correlation function values obtained from a third order spline calculation. Secondly, the angular step of the correlation histogram must be smaller than the map step, otherwise some information is lost. For instance, at small separation angle, it is necessary to distinguish the angular separation angle of adjacent cells from the one of cells which are neighbours on a diagonal. We have used a sampling four times finer than the interval between adjacent map cells ( $\frac{1}{4} \text{ arcmin}$ ).

With these cautions, reconstructed  $C_l$  are shown in figure 17 and 18. The filter shapes have been chosen according to the discussion of the preceding section. Figure 17 shows



the average of the reconstructed  $C_l$  spectra over the 173 simulated maps, while figure 18 shows one particular simulation. Figure 17 compares also the calculated variance of the  $C_l$  (formula V.27) with the variance deduced from the 173 simulations. They agree well for  $l \lesssim 1500$ . The discrepancy at larger  $l$  values may be due to the HEALPIX map resolution, and to the histogram binwidth definition. This is reflected by the systematic bias of the average reconstructed  $C_l$  spectrum for  $l > 2200$ . Figure 18 compares the reconstructed  $C_l$  spectra obtained with two different apodisation cut-off parameters. The one corresponding to  $\theta_0 = 5 \text{ deg}$  looks better than the one obtained with  $\theta_0 = 10 \text{ deg}$ , but this reflects only the fact that the  $C_l$  values are correlated on a larger scale in the first case, washing out some fluctuations, as shown in figure 19.

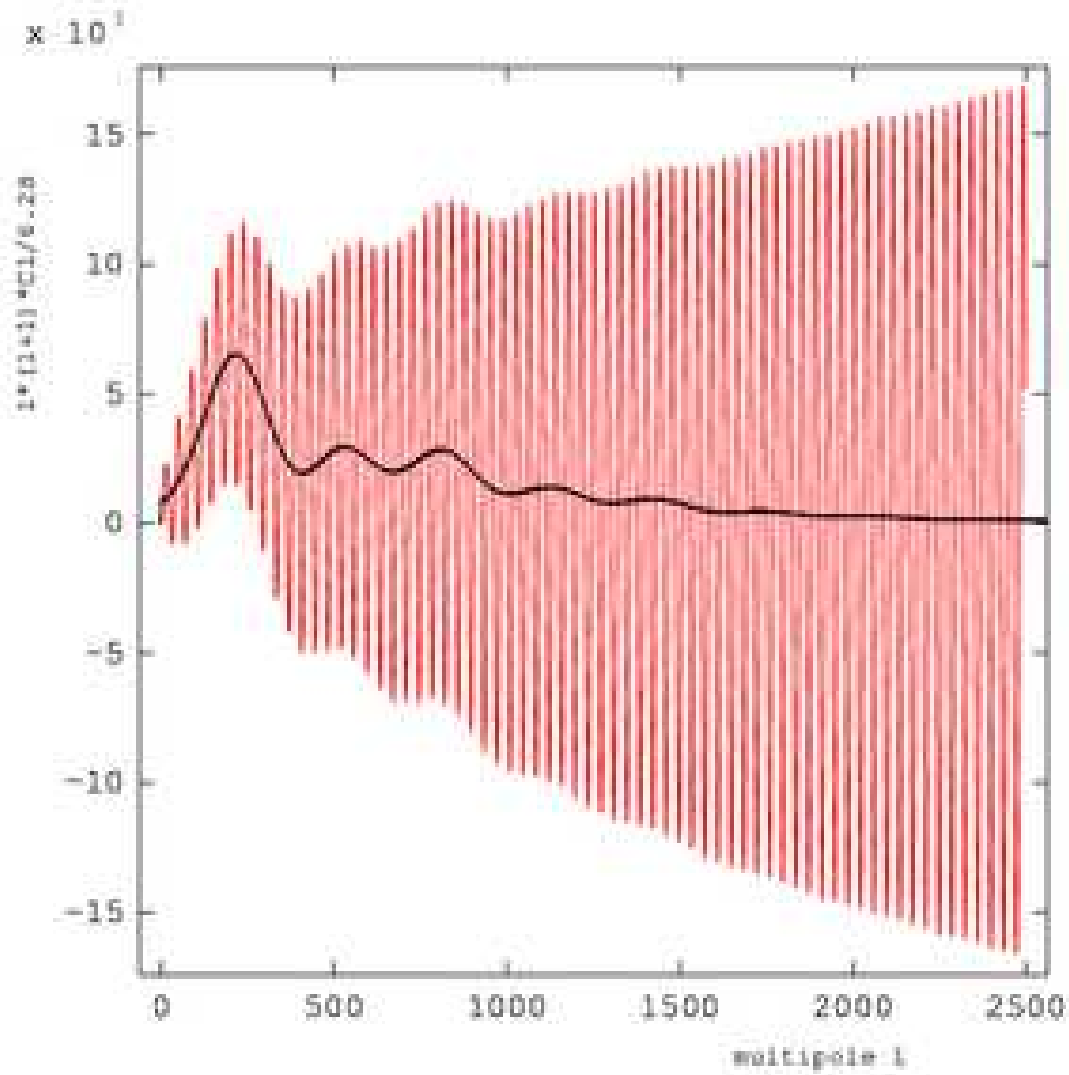


Figure 13: Predicted  $\langle \tilde{C}_l^\xi \rangle$  from  $\tilde{\xi}(\gamma)$  integration for a spherical cap of aperture  $19 \text{ deg}$ :  
- the red curve shows the predicted  $l(l+1) \langle \tilde{C}_l^\xi \rangle / 2\pi$   
- the black curve the input  $l(l+1)C_l/2\pi$  spectrum.

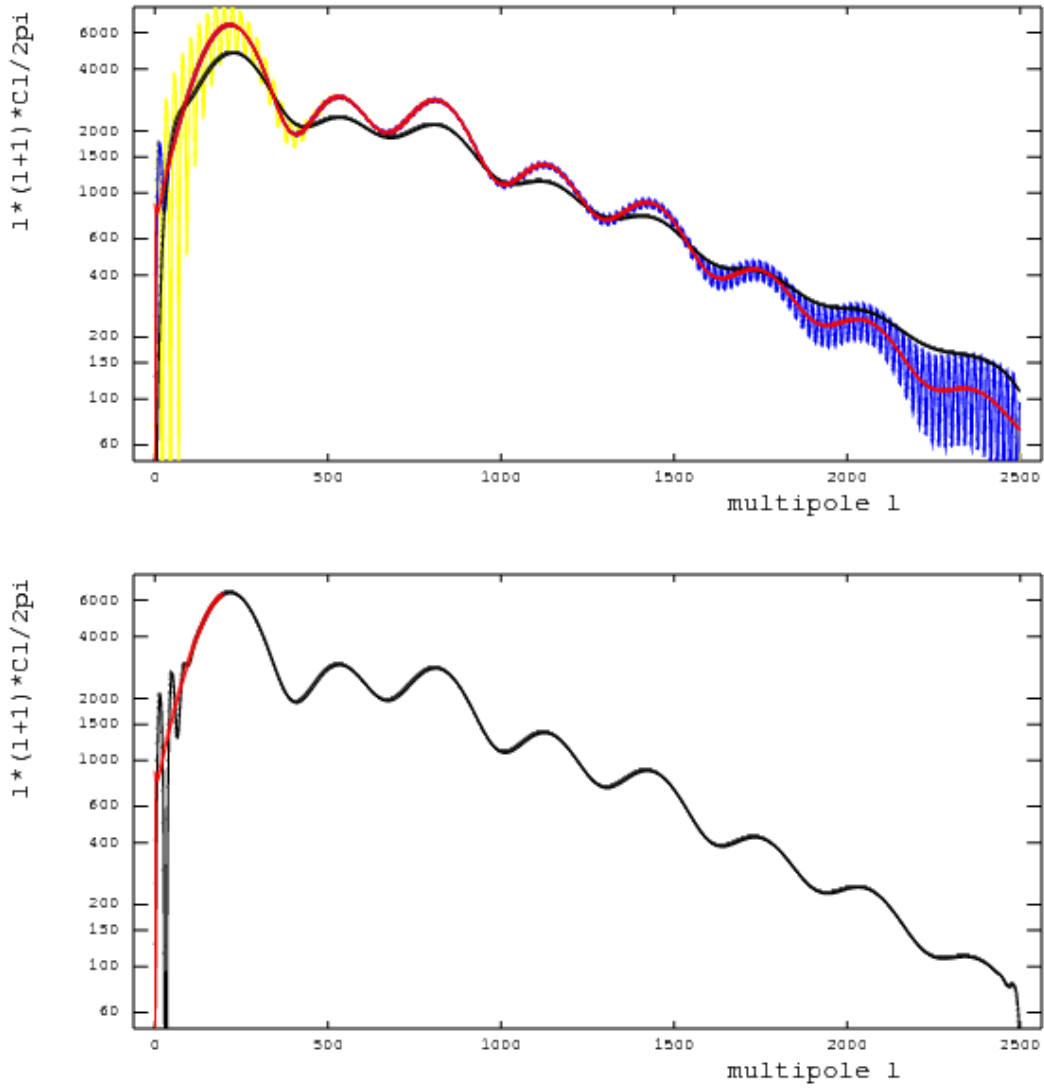


Figure 14: Predicted  $l(l + 1) \langle \tilde{C}_l^\xi \rangle$  from  $\tilde{\xi}(\gamma)$  integration with apodization for a spherical cap of aperture  $19 \text{ deg}$ :

- *Top figure*

- the yellow curve is for apodization ( $\theta_0 = 15 \text{ deg}$ ,  $\Delta = 0.5 \text{ deg}$ )

- the blue curve is for apodization ( $\theta_0 = 10 \text{ deg}$ ,  $\Delta = 5 \text{ deg}$ )

- the black curve is for apodization ( $\theta_0 = 1 \text{ deg}$ ,  $\Delta = 2 \text{ deg}$ )

- the red curve is the  $l(l + 1)C_l/2\pi$  input spectrum (the curve is undistinguishable from the yellow one at large  $l$ ).

- *Bottom figure*

- the black curve is for apodization ( $\theta_0 = 10 \text{ deg}$ ,  $\Delta = 2 \text{ deg}$ )

- the red curve is the  $l(l + 1)C_l/2\pi$  input spectrum (the curve is not plotted above  $l = 200$  because it is undistinguishable from the black one).

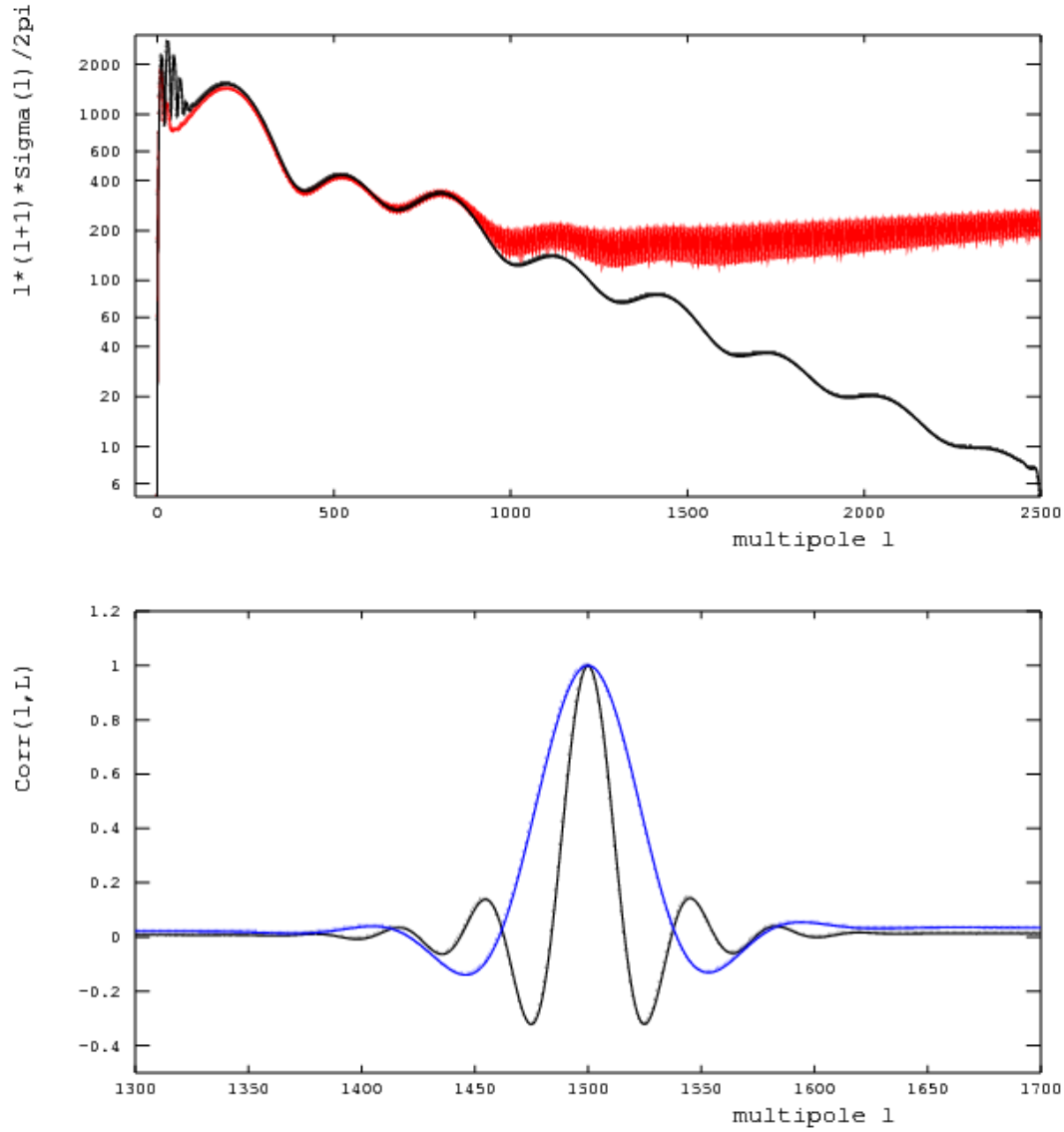


Figure 15: Predicted variance and correlation for  $\tilde{C}_l^\xi$  with apodization for a spherical cap of aperture 19 deg:

- *Top figure:*  $l(l+1)\sigma_{\tilde{C}_l^\xi}/2\pi$ 
  - the black curve is for apodization ( $\theta_0 = 10$  deg,  $\Delta = 2$  deg)
  - the red curve is for apodization ( $\theta_0 = 10$  deg,  $\Delta = 5$  deg)
- *Bottom figure:* correlation values for  $l = 1500$ 
  - the black curve is for apodization ( $\theta_0 = 10$  deg,  $\Delta = 2$  deg)
  - the blue curve is for apodization ( $\theta_0 = 5$  deg,  $\Delta = 2$  deg)

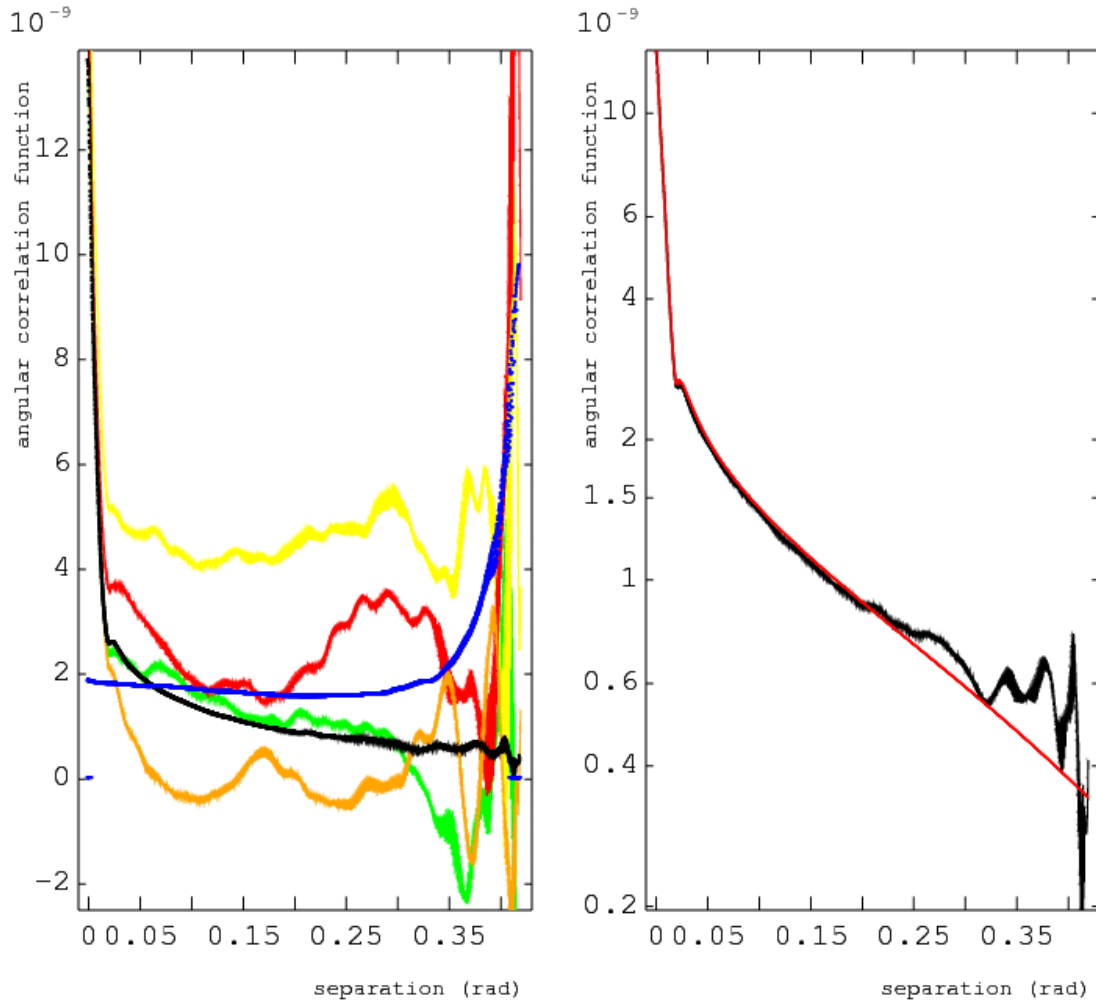


Figure 16: Reconstructed angular correlation function from 173 simulations of  $17 \text{ deg} \times 17 \text{ deg}$  squared maps:

- *Left figure*

- the yellow, orange, green and red curves are reconstructed angular function on 4 individual generations.

- the black curve is the mean angular function computed from the 173 generations.

- the blue curve is the dispersion of the angular functions computed from the 173 generations.

- *Right figure*

- the black curve is the mean angular function computed from the 173 generations.

- the red curve is the expected angular function computed directly from the input  $C_l$  spectrum

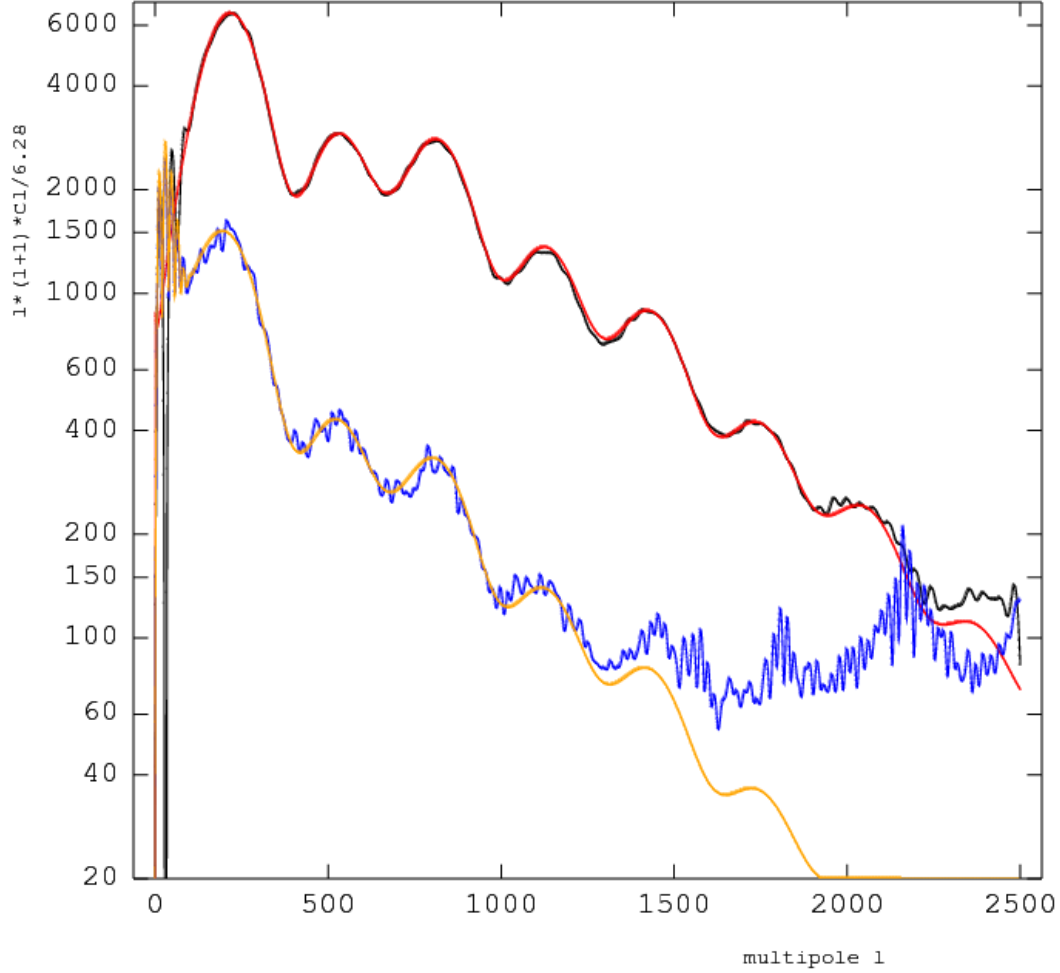


Figure 17: Reconstructed  $l(l+1) \langle \tilde{C}_l^\xi \rangle / 2\pi$  from  $\tilde{\xi}(\gamma)$  integration with apodization on 173 simulations of  $17 \text{ deg} \times 17 \text{ deg}$  squared maps:

- the black curve shows the mean reconstructed  $l(l+1) \langle \tilde{C}_l^\xi \rangle / 2\pi$  for apodization ( $\theta_0 = 10 \text{ deg}$ ,  $\Delta = 2 \text{ deg}$ )
- the red curve shows the  $l(l+1)C_l/2\pi$  input spectrum
- the blue curve shows the dispersion  $\sigma_{\tilde{C}_l^\xi}$  of the reconstructed  $\tilde{C}_l^\xi$  on the generations for the same apodization
- the orange curve shows the dispersion  $\sigma_{\tilde{C}_l^\xi}$  predicted by (V.27) and (V.30) for a  $17 \times 17 \text{ deg}^2$  spherical cap

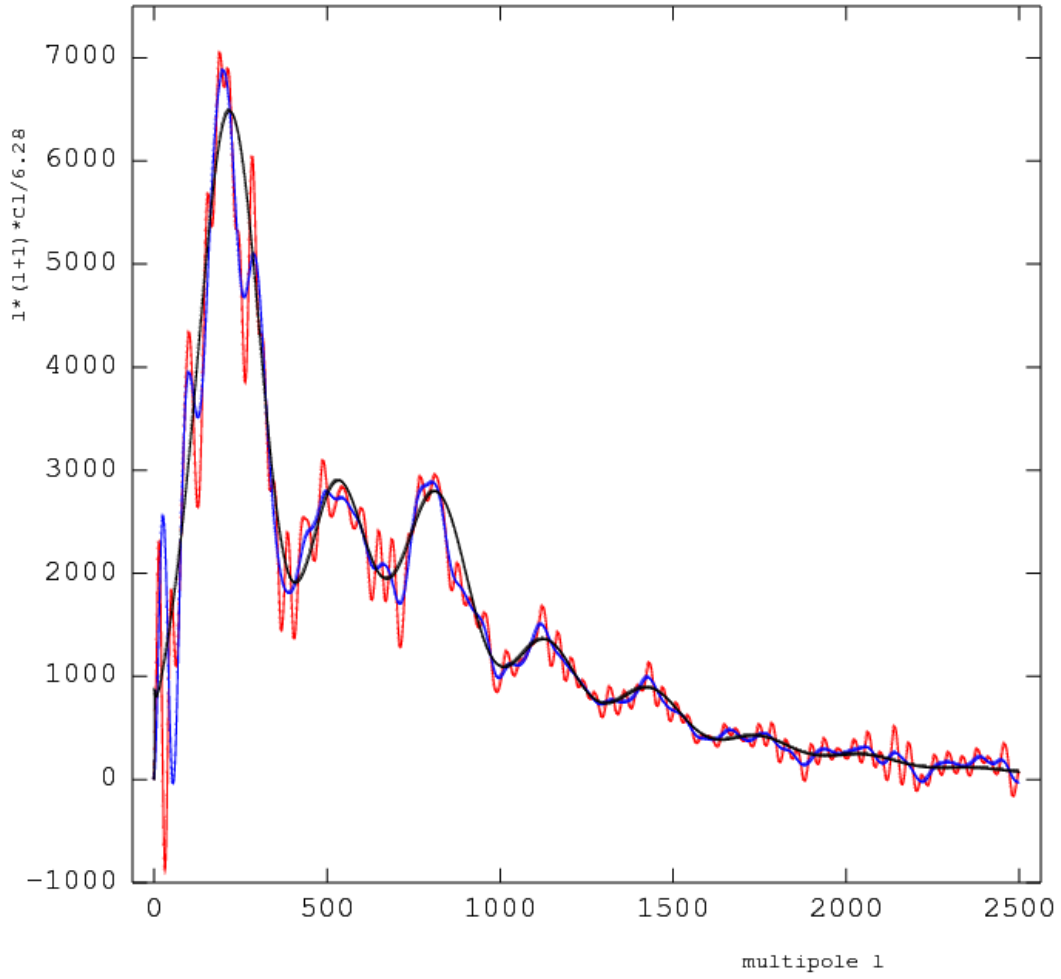


Figure 18: Reconstructed  $l(l+1)\tilde{C}_l^\xi/2\pi$  for integration with apodization for one individual generation of a  $17 \text{ deg} \times 17 \text{ deg}$  squared map:

- the red curve is for apodization ( $\theta_0 = 10 \text{ deg}$ ,  $\Delta = 2 \text{ deg}$ )
- the blue curve is for apodization ( $\theta_0 = 5 \text{ deg}$ ,  $\Delta = 2 \text{ deg}$ )
- the black curve shows the  $l(l+1)C_l/2\pi$  input spectrum

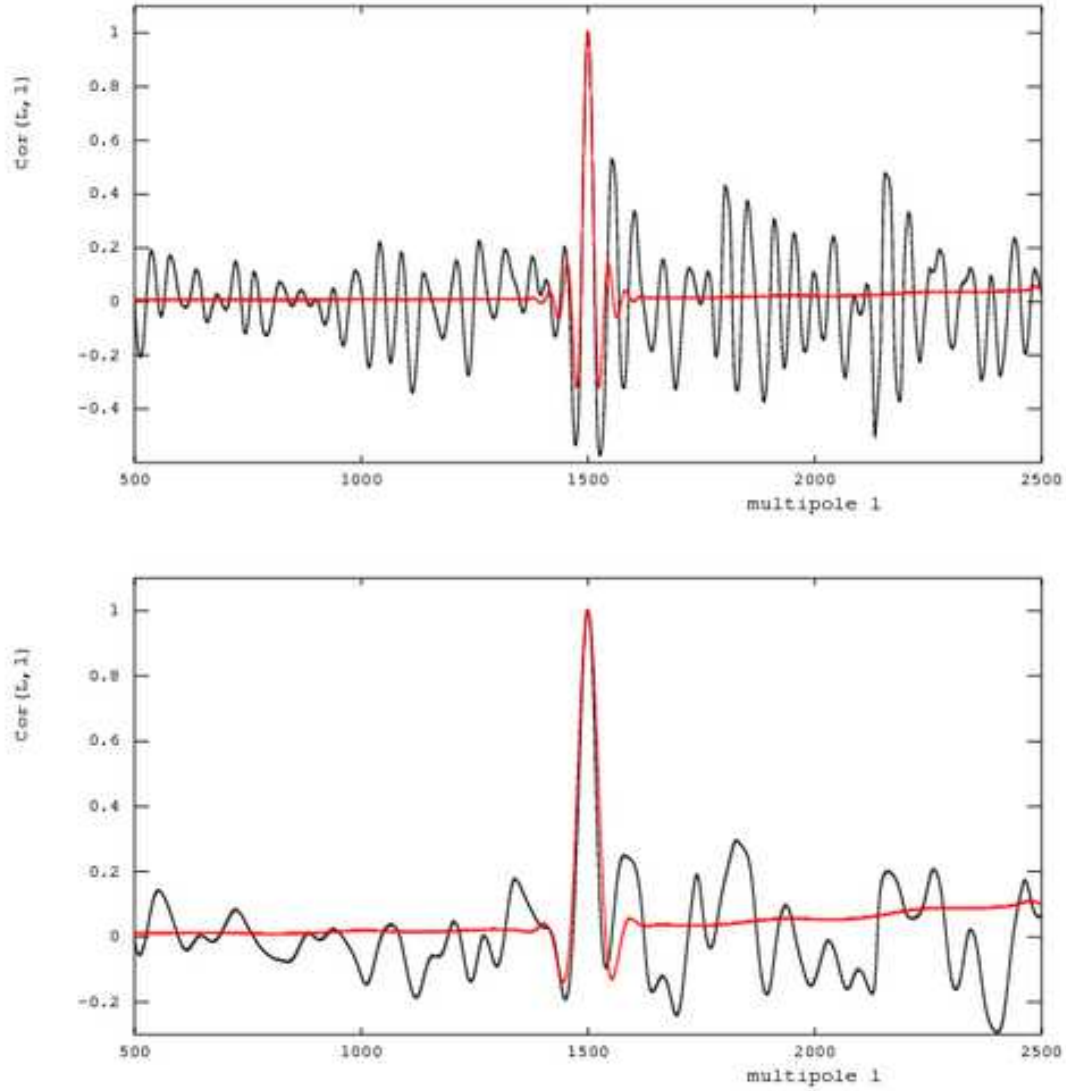


Figure 19: Reconstructed correlation of  $\tilde{C}_l^\xi$  for integration with apodization for  $L = 1500$ :  
- *Top figure* is for apodization ( $\theta_0 = 10 \text{ deg}$ ,  $\Delta = 2 \text{ deg}$ )  
- *Bottom figure* is for apodization ( $\theta_0 = 5 \text{ deg}$ ,  $\Delta = 2 \text{ deg}$ )  
- black curves are the reconstructed  $Cor(l, L)$  on the 173 generations of  $17 \text{ deg} \times 17 \text{ deg}$  squared maps  
- red curves are the predicted  $Cor(l, L)$  for a  $17 \times 17 \text{ deg}^2$  spherical cap



## VI Conclusion.

In these notes we have computed the biases and covariance of the  $C_l$  reconstructed from small sky maps. This was done for two methods, the widely used one based on FFT analysis of the temperature field, and the one which uses the angular correlation spectrum. These two methods are complementary. Estimators of the  $C_l$  have been defined and we have shown how they can be computed numerically, as well as their covariance matrix and correlations. These calculations are simpler to perform in the case of spherical cap maps, due to the high degree of symmetry. We have shown, using simulated sky maps, that most of the results do not depend on the map shape at first order. Most of the biases introduced by the use of small maps can be studied numerically without having to simulate large amounts of sky maps. We have also studied the complicated dependency of the reconstructed  $C_l$  variance over the map size. In the case of the correlation spectrum we have shown how its apodisation works.

# APPENDICES

## A Computation of the angular correlation integral.

Let's compute the internal integral  $\mathcal{I}$  of the angular correlation function of section ii.3:

$$\mathcal{I} = \int_{S^2 \times S^2} \overline{Y_{l_1}^{m_1}}(\Omega_1) Y_{l_2}^{m_2}(\Omega_2) d\Omega_1 d\Omega_2 \delta(\vec{\Omega}_1 \cdot \vec{\Omega}_2 - \cos(\gamma))$$

We rotate the original coordinate axis  $Oxyz$  to  $OXYZ$  such that  $\vec{\Omega}_1 = (\theta_1, \phi_1)$  be the unit vector along  $OZ$ . Such a rotation is performed by first rotating by an angle  $\phi_1$  around  $Oz$ . The  $Oy$  axis moves to  $Oy_1$ . Then a rotation with angle  $\theta_1$  around  $Oy_1$  is performed. The rotation which transforms  $Oxyz$  to  $OXYZ$  is the rotation of Euler angles  $R(\alpha = \phi_1, \beta = \theta_1, 0)$ . Let's  $(\theta_2, \phi_2)$  be the coordinates of  $\vec{\Omega}_2$  in  $Oxyz$  et  $(\Theta_2, \Phi_2)$  in  $OXYZ$ .

The transformation law of the spherical harmonics is (see [Messiah, 1964]):

$$Y_{l_2}^{m_2}(\Theta_2, \Phi_2) = \sum_{m'_2} Y_{l_2}^{m'_2}(\theta_2, \phi_2) \mathfrak{D}_{m'_2 m_2}^{(l_2)}(R(\phi_1, \theta_1))$$

The inverse rotation gives:

$$Y_{l_2}^{m_2}(\theta_2, \phi_2) = \sum_{m'_2} Y_{l_2}^{m'_2}(\Theta_2, \Phi_2) \mathfrak{D}_{m'_2 m_2}^{(l_2)}(R^{-1}(\phi_1, \theta_1))$$

As  $R$  is a unitary transform  $\mathfrak{D}_{m' m}^{(l)}(R^{-1}(\phi, \theta)) = \overline{\mathfrak{D}_{m m'}^{(l)}(R(\phi, \theta))}$  so we obtain:

$$Y_{l_2}^{m_2}(\theta_2, \phi_2) = \sum_{m'_2} Y_{l_2}^{m'_2}(\Theta_2, \Phi_2) \overline{\mathfrak{D}_{m_2 m'_2}^{(l_2)}(R(\phi_1, \theta_1))}$$

Let's go back to  $\mathcal{I}$ . As the transform is a rotation, the jacobian is equal to 1 and:

$$d\Omega_1 d\Omega_2 = d \cos(\theta_1) d\phi_1 d \cos(\theta_2) d\phi_2 = d \cos(\theta_1) d\phi_1 d \cos(\Theta_2) d\Phi_2$$

The scalar product is invariant under rotation, so the argument of the delta distribution remains unchanged:  $\vec{\Omega}_1 \cdot \vec{\Omega}_2 = \cos(\Theta_2)$ .

$$\begin{aligned} \mathcal{I} &= \int_{S^2 \times S^2} \overline{Y_{l_1}^{m_1}}(\theta_1, \phi_1) \sum_{m'_2} Y_{l_2}^{m'_2}(\Theta_2, \Phi_2) \overline{\mathfrak{D}_{m_2 m'_2}^{(l_2)}(R(\phi_1, \theta_1))} d \cos(\theta_1) d\phi_1 d \cos(\Theta_2) d\Phi_2 \\ &\quad \delta(\cos(\Theta_2) - \cos(\gamma)) \\ &= \int_{S^2 \times S^2} \overline{Y_{l_1}^{m_1}}(\theta_1, \phi_1) \sum_{m'_2} Y_{l_2}^{m'_2}(\gamma, \Phi_2) \overline{\mathfrak{D}_{m_2 m'_2}^{(l_2)}(R(\phi_1, \theta_1))} d \cos(\theta_1) d\phi_1 d\Phi_2 \end{aligned}$$

Since  $Y_{l_2}^{m'_2}(\gamma, \Phi_2) = \sqrt{\frac{2l+1}{4\pi} \frac{(l_2-m'_2)!}{(l_2+m'_2)!}} P_{l_2}^{m'_2}(\cos(\gamma)) e^{im'_2\Phi_2}$ ,  
for the integral over  $\Phi_2$  to be non zero, we must have  $m'_2 = 0$ .

$$\mathcal{I} = \int_{S^2} \overline{Y_{l_1}^{m_1}}(\theta_1, \phi_1) \sqrt{\frac{2l+1}{4\pi}} P_{l_2}^0(\cos(\gamma)) \overline{\mathfrak{D}_{m_2 0}^{(l_2)}}(R(\phi_1, \theta_1)) 2\pi d \cos(\theta_1) d\phi_1$$

with

$$\mathfrak{D}_{m_2 0}^{(l_2)}(R(\phi_1, \theta_1)) = \sqrt{\frac{4\pi}{2l+1}} Y_{l_2}^{m_2}(\theta_1, \phi_1)$$

and  $P_{l_2}^0(\cos(\gamma)) = P_{l_2}(\cos(\gamma))$ , we obtain:

$$\begin{aligned} \mathcal{I} &= \int_{S^2} \overline{Y_{l_1}^{m_1}}(\theta_1, \phi_1) \sqrt{\frac{4\pi}{2l+1}} Y_{l_2}^{m_2}(\theta_1, \phi_1) \sqrt{\frac{2l+1}{4\pi}} P_{l_2}(\cos(\gamma)) 2\pi d \cos(\theta_1) d\phi_1 \\ &= 2\pi \delta_{l_1 l_2} \delta_{m_1 m_2} P_{l_2}(\cos(\gamma)) \end{aligned}$$

$$\mathcal{I} = 2\pi \delta_{l_1 l_2} \delta_{m_1 m_2} P_{l_2}(\cos(\gamma)) \tag{A.1}$$

## B Computation of the $\tilde{C}_l$ covariance for a portion of sphere.

We have seen (cf section iii.2) that we can write:

$$\tilde{a}_{lm} = \sum_{l'm'} B_{lm;l'm'} a_{l'm'}$$

with either

$$B_{lm;l'm'} = (-1)^m \sum_{l'',m''} b_{l''m''} \sqrt{\frac{(2l+1)(2l'+1)(2l''+1)}{4\pi}} \begin{pmatrix} l' & l & l'' \\ m' & -m & m'' \end{pmatrix} \begin{pmatrix} l' & l & l'' \\ 0 & 0 & 0 \end{pmatrix}$$

or

$$B_{lm;l'm'} = \int_A Y_l^{m'} \overline{Y_l^m} d\Omega$$

The relation  $\overline{Y_l^{-m}} = (-1)^m Y_l^m$  leads to:

$$\overline{B_{lm;l'm'}} = B_{l'm';lm} = (-1)^{m+m'} B_{l-m;l'-m'} \in \mathbb{C}$$

► Let's compute the ensemble average  $\langle \tilde{C}_l \rangle$ :

$$\begin{aligned} \tilde{C}_l &= \frac{1}{2l+1} \sum_{m=-l}^{+l} \overline{\tilde{a}_{lm}} \tilde{a}_{lm} \\ &= \frac{1}{2l+1} \sum_m \sum_{l'm'} \sum_{l''m''} \overline{B_{lm;l'm'}} B_{lm;l''m''} \overline{a_{l'm'}} a_{l''m''} \\ \langle \tilde{C}_l \rangle &= \frac{1}{2l+1} \sum_m \sum_{l'm'} \sum_{l''m''} \overline{B_{lm;l'm'}} B_{lm;l''m''} \langle \overline{a_{l'm'}} a_{l''m''} \rangle \\ &= \frac{1}{2l+1} \sum_m \sum_{l'm'} \sum_{l''m''} \overline{B_{lm;l'm'}} B_{lm;l''m''} \delta_{l'l''} \delta_{m'm''} C_l \end{aligned}$$

$$\langle \tilde{C}_l \rangle = \frac{1}{2l+1} \sum_{m=-l}^{+l} \sum_{l'm'} |B_{lm;l'm'}|^2 C_l$$

► Now let's compute the  $\tilde{C}_l$  covariance:

$$\tilde{C}_l \overline{\tilde{C}_L} = \frac{1}{(2l+1)(2L+1)} \sum_m \sum_{l'm'} \sum_{l''m''} \sum_M \sum_{L'M'} \sum_{L''M''} \overline{B_{lm;l'm'}} \overline{B_{lm;l''m''}} \overline{B_{LM;L'M'}} \overline{B_{LM;L''M''}} a_{l'm'} \overline{a_{l''m''}} a_{L'M'} \overline{a_{L''M''}}$$

Using the ensemble average of 4  $a_{lm}$  products for a *real gaussian* temperature field:

$$\begin{aligned} \langle a_{l_1 m_1} \overline{a_{l_2 m_2}} a_{l_3 m_3} \overline{a_{l_4 m_4}} \rangle &= C_{l_1} C_{l_3} (\delta_{l_1 l_2} \delta_{m_1 m_2} \delta_{l_3 l_4} \delta_{m_3 m_4} + \delta_{l_1 l_4} \delta_{m_1 m_4} \delta_{l_2 l_3} \delta_{m_2 m_3}) \\ &\quad + (-1)^{m_1+m_2} C_{l_1} C_{l_2} \delta_{l_1 l_3} \delta_{m_1-m_3} \delta_{l_2 l_4} \delta_{m_2-m_4} \end{aligned}$$

We obtain:

$$\begin{aligned}
\langle \tilde{C}_l \tilde{C}_L \rangle &= \frac{1}{(2l+1)(2L+1)} \sum \cdots \sum B_{lm;l'm'} \overline{B_{lm;l'm''}} B_{LM;L'M'} \overline{B_{LM;L'M''}} \\
&\quad \{ C_{l'} C_{L'} (\delta_{l'l''} \delta_{m'm''} \delta_{L'L''} \delta_{M'M''} + \delta_{l'L''} \delta_{m'M''} \delta_{l''L'} \delta_{m''M'}) \\
&\quad + (-1)^{m'+m''} C_{l'} C_{l''} \delta_{l'L'} \delta_{m'-M'} \delta_{l''L''} \delta_{m''-M''} \} \\
\langle \tilde{C}_l \overline{\tilde{C}_L} \rangle &= \frac{1}{(2l+1)(2L+1)} \sum_m \sum_M \{ \\
&\quad \sum_{l'm'L'M'} C_{l'} C_{L'} B_{lm;l'm'} \overline{B_{lm;l'm'}} B_{LM;L'M'} \overline{B_{LM;L'M'}} \\
&\quad + \sum_{l'm'L'M'} C_{l'} C_{L'} B_{lm;l'm'} \overline{B_{lm;L'M'}} B_{LM;L'M'} \overline{B_{LM;l'm'}} \\
&\quad + (-1)^{m'+m''} \sum_{l'm'l''m''} C_{l'} C_{l''} B_{lm;l'm'} \overline{B_{lm;l''m''}} B_{LM;l'-m'} \overline{B_{LM;l''-m''}} \\
&\quad \}
\end{aligned}$$

The first term corresponds to  $\langle \tilde{C}_l \rangle \langle \tilde{C}_L \rangle$ .

One could exchange  $l'', m''$  to  $L', M'$  in the third term sum:

$$\begin{aligned}
V(l, L) &= \langle \tilde{C}_l \tilde{C}_L \rangle - \langle \tilde{C}_l \rangle \langle \tilde{C}_L \rangle \\
&= \frac{1}{(2l+1)(2L+1)} \sum_m \sum_M \sum_{l'm'} \sum_{L'M'} C_{l'} C_{L'} \{ \\
&\quad B_{lm;l'm'} \overline{B_{lm;L'M'}} B_{LM;L'M'} \overline{B_{LM;l'm'}} \\
&\quad + (-1)^{m'+M'} B_{lm;l'm'} \overline{B_{lm;L'M'}} B_{LM;l'-m'} \overline{B_{LM;L'-M'}} \\
&\quad \}
\end{aligned}$$

Then exchanging  $M$  to  $-M$  in the second term sum and using the symmetry relation for the  $B_{lm;l'm'}$ :

$$\begin{aligned}
V(l, L) &= \frac{1}{(2l+1)(2L+1)} \sum_m \sum_M \sum_{l'm'} \sum_{L'M'} C_{l'} C_{L'} \{ \\
&\quad B_{lm;l'm'} \overline{B_{lm;L'M'}} B_{LM;L'M'} \overline{B_{LM;l'm'}} \\
&\quad + (-1)^{m'+M'} B_{lm;l'm'} \overline{B_{lm;L'M'}} B_{L-M;l'-m'} \overline{B_{L-M;L'-M'}} \\
&\quad \} \\
&= \frac{1}{(2l+1)(2L+1)} \sum_m \sum_M \sum_{l'm'} \sum_{L'M'} C_{l'} C_{L'} \{ \\
&\quad B_{lm;l'm'} \overline{B_{lm;L'M'}} B_{LM;L'M'} \overline{B_{LM;l'm'}} \\
&\quad + B_{lm;l'm'} \overline{B_{lm;L'M'}} \overline{B_{LM;l'm'}} B_{LM;L'M'} \\
&\quad \} \\
&= \frac{2}{(2l+1)(2L+1)} \sum_m \sum_M \sum_{l'm'} \sum_{L'M'} C_{l'} C_{L'} \{ \\
&\quad B_{lm;l'm'} \overline{B_{lm;L'M'}} B_{LM;L'M'} \overline{B_{LM;l'm'}} \\
&\quad \} \\
&= \frac{2}{(2l+1)(2L+1)} \sum_m \sum_M \left( \sum_{l'm'} C_{l'} B_{lm;l'm'} \overline{B_{LM;l'm'}} \right) \left( \sum_{L'M'} C_{L'} \overline{B_{lm;L'M'}} B_{LM;L'M'} \right) \\
&= \frac{2}{(2l+1)(2L+1)} \sum_m \sum_M \left( \sum_{l'm'} C_{l'} B_{lm;l'm'} \overline{B_{LM;l'm'}} \right) \left( \sum_{L'M'} C_{L'} B_{lm;L'M'} \overline{B_{LM;L'M'}} \right)
\end{aligned}$$

We finally obtain:

$$\begin{aligned}
V(l, L) &= \langle \tilde{C}_l \tilde{C}_L \rangle - \langle \tilde{C}_l \rangle \langle \tilde{C}_L \rangle \\
&= \frac{2}{(2l+1)(2L+1)} \sum_{m=-l}^{+l} \sum_{M=-L}^{+L} \left| \sum_{l'm'} C_{l'} B_{lm;l'm'} \overline{B_{LM;l'm'}} \right|^2
\end{aligned}$$

If we replace the  $B_{lm;l'm'}$  by their values, we obtain:

$$\begin{aligned}
V(l, L) &= \frac{2}{(2l+1)(2L+1)} \sum_{m=-l}^{+l} \sum_{M=-L}^{+L} \left| \sum_{l'm'} C_{l'} \right. \\
&\times \left[ \sum_{b\beta} b_{b\beta} (-1)^m \sqrt{\frac{(2l+1)(2l'+1)(2b+1)}{4\pi}} \begin{pmatrix} l' & l & b \\ m' & -m & \beta \end{pmatrix} \begin{pmatrix} l' & l & b \\ 0 & 0 & 0 \end{pmatrix} \right] \\
&\times \left[ \sum_{d\delta} \overline{b_{d\delta}} (-1)^M \sqrt{\frac{(2L+1)(2l'+1)(2d+1)}{4\pi}} \begin{pmatrix} l' & L & d \\ m' & -M & \delta \end{pmatrix} \begin{pmatrix} l' & L & d \\ 0 & 0 & 0 \end{pmatrix} \right] \Big|^2 \\
&= \frac{2}{(4\pi)^2} \sum_{m=-l}^{+l} \sum_{M=-L}^{+L} \left| \sum_{l'm'} (2l'+1) C_{l'} \times \sum_{b\beta} \sum_{d\delta} \sqrt{(2b+1)(2d+1)} b_{b\beta} \overline{b_{d\delta}} \right. \\
&\quad \times \begin{pmatrix} l' & l & b \\ m' & -m & \beta \end{pmatrix} \begin{pmatrix} l' & L & d \\ m' & -M & \delta \end{pmatrix} \begin{pmatrix} l' & l & b \\ 0 & 0 & 0 \end{pmatrix} \begin{pmatrix} l' & L & d \\ 0 & 0 & 0 \end{pmatrix} \Big|^2
\end{aligned}$$

That formula is not very usefull because it involves the computation of a general  $3j$  symbol which is time consuming. This is why we have to add another constraint: *the spherical symetry of the portion of sphere under study.*

Note that we would have obtain exactly the same result by doing the computation with the other definition for the  $B_{lm;l'm'}$ . In this case, because it would involve integral of product of  $Y_l^m$  other a portion of sphere of general shape, the computation time would be enormous .

## C Computation of the angular correlation distribution

### for a portion of sphere.

Let's compute

$$\begin{aligned} \mathcal{N}^A(\gamma) \tilde{\xi}(\gamma) &= \sum_{\dots} \overline{a_{l_1 m_1}} \overline{b_{L_1 M_1}} a_{l_2 m_2} b_{L_2 M_2} \\ &\quad \times \int_{S^2 \times S^2} d\Omega_1 d\Omega_2 \delta(\vec{\Omega}_1 \cdot \vec{\Omega}_2 - \cos(\gamma)) \overline{Y_{l_1}^{m_1}}(\Omega_1) \overline{Y_{L_1}^{M_1}}(\Omega_1) Y_{l_2}^{m_2}(\Omega_2) Y_{L_2}^{M_2}(\Omega_2) \end{aligned}$$

where the sum  $\sum$  runs on  $\{l_1, m_1, L_1, M_1, l_2, m_2, L_2, M_2\}$ .

We perform the integration on  $\Omega_2$  by rotating the frame  $(Oxyz)$  into  $(Ox'y'z')$  such that the axis  $Oz'$  be on  $\vec{\Omega}_1$  (see figure 20)

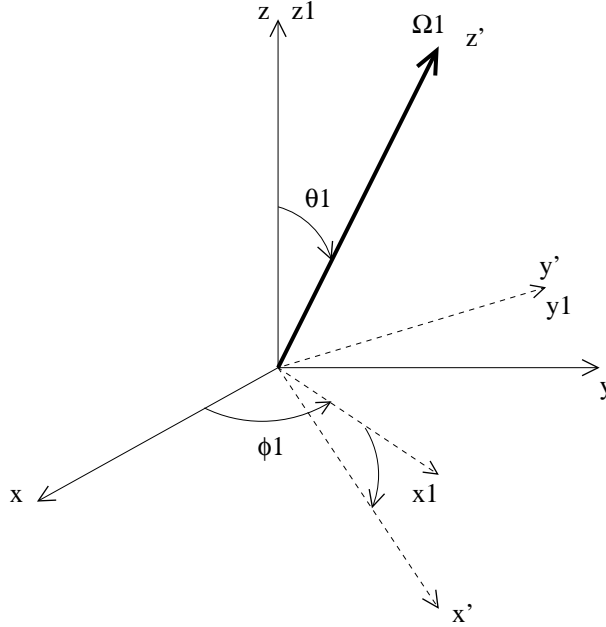


Figure 20: Euler rotation.

We perform the Euler rotation  $R(\alpha, \beta, \gamma)$  of the frame<sup>6</sup>:

- Rotation of  $\alpha = \phi_1$  around  $Oz$ :  $(O, x, y, z) \rightarrow (O, x_1, y_1, z_1 = z)$
- Rotation of  $\beta = \theta_1$  around  $Oy_1$ :  $(O, x_1, y_1, z_1 = z) \rightarrow (O, x', y' = y_1, z')$
- Rotation of  $\gamma = 0$  around  $Oz_2$  (i.e. the identity).

So the rotation is:  $R(\alpha, \beta, \gamma) = R(\phi_1, \theta_1, 0)$ .

We define  $(\theta, \phi)$  to be the polar coordinates of the frame  $(O, x, y, z)$  and  $(\theta', \phi')$  the polar

---

<sup>6</sup> Here  $\gamma$  is the third angle of the Euler rotation not the separation angle of the angular correlation function.

coordinates in the new frame  $(O, x', y', z')$ .

$$\begin{aligned} Y_l^m(\theta', \phi') &= \sum_{m'} \mathfrak{D}_{m'm}^{(l)}(\phi_1, \theta_1, 0) Y_l^{m'}(\theta, \phi) \\ Y_l^m(\theta, \phi) &= \sum_{m'} \overline{\mathfrak{D}_{mm'}^{(l)}}(\phi_1, \theta_1, 0) Y_l^{m'}(\theta', \phi') \end{aligned}$$

Performing the rotation we get:

$$\begin{aligned} \mathcal{N}^A(\gamma) \tilde{\xi}(\gamma) &= \sum_{\dots} \overline{a_{l_1 m_1}} \overline{b_{L_1 M_1}} a_{l_2 m_2} b_{L_2 M_2} \int_{S^2} d\Omega_1 \overline{Y_{l_1}^{m_1}}(\Omega_1) \overline{Y_{L_1}^{M_1}}(\Omega_1) \\ &\quad \times \int_{S^2} d\Omega'_2 \delta(\vec{\Omega}'_1 \cdot \vec{\Omega}'_2 - \cos(\gamma)) \overline{\mathfrak{D}_{m_2 m'_2}^{(l_2)}} Y_{l_2}^{m'_2}(\Omega'_2) \overline{\mathfrak{D}_{M_2 M'_2}^{(L_2)}} Y_{L_2}^{M'_2}(\Omega'_2) \end{aligned}$$

where the sum runs on  $\{l_1, m_1, L_1, M_1, l_2, m_2, L_2, M_2, m'_2, M'_2\}$

and where we simplify the notation  $\mathfrak{D}_{m'm}^{(l)} \equiv \mathfrak{D}_{m'm}^{(l)}(\phi_1, \theta_1, 0)$ .

We have  $d\Omega'_2 = d\cos(\theta'_2) d\phi'_2$ . The integral on  $d\cos(\theta'_2)$  and the function  $\delta(\dots)$  leads to the replacement of  $\theta'_2$  by  $\gamma$ . Writing  $Y_l^m(\theta, \phi) = \lambda_l^m(\theta) e^{im\phi}$ , we have for the integral on  $\phi'_2$ :

$$\begin{aligned} \int_0^\pi \int_0^{2\pi} d\cos(\theta'_2) d\phi'_2 Y_{l_2}^{m'_2}(\Omega'_2) Y_{L_2}^{M'_2}(\Omega'_2) &= \int_0^{2\pi} d\phi'_2 \lambda_{l_2}^{m'_2}(\gamma) \lambda_{L_2}^{M'_2}(\gamma) e^{i(m'_2 + M'_2)\phi'_2} \\ &= 2\pi \delta_{m'_2, -M'_2} \lambda_{l_2}^{m'_2}(\gamma) \lambda_{L_2}^{M'_2}(\gamma) \end{aligned}$$

Thus we obtain:

$$\begin{aligned} \mathcal{N}^A(\gamma) \tilde{\xi}(\gamma) &= 2\pi \sum_{\dots} \overline{a_{l_1 m_1}} a_{l_2 m_2} \overline{b_{L_1 M_1}} b_{L_2 M_2} \lambda_{l_2}^{m'_2}(\gamma) \lambda_{L_2}^{-m'_2}(\gamma) \\ &\quad \times \int_{S^2} d\Omega_1 \overline{Y_{l_1}^{m_1}}(\Omega_1) \overline{Y_{L_1}^{M_1}}(\Omega_1) \overline{\mathfrak{D}_{m_2 m'_2}^{(l_2)}} \overline{\mathfrak{D}_{M_2 - m'_2}^{(L_2)}} \end{aligned}$$

where the sum runs on  $\{l_1, m_1, L_1, M_1, l_2, m_2, L_2, M_2, m'_2\}$ .

Now we perform the ensemble average, and as  $\langle \overline{a_{l_1 m_1}} a_{l_2 m_2} \rangle = C_{l_1} \delta_{l_1 l_2} \delta_{m_1 m_2}$ , we get:

$$\begin{aligned} \langle \mathcal{N}^A(\gamma) \tilde{\xi}(\gamma) \rangle &= 2\pi \sum_{\dots} \overline{b_{L_1 M_1}} b_{L_2 M_2} C_{l_1} \lambda_{l_1}^{m'_2}(\gamma) \lambda_{L_2}^{-m'_2}(\gamma) \\ &\quad \times \int_{S^2} d\Omega_1 \overline{\mathfrak{D}_{m_1 m'_2}^{(l_1)}} \overline{Y_{l_1}^{m_1}}(\Omega_1) \overline{\mathfrak{D}_{M_2 - m'_2}^{(L_2)}} \overline{Y_{L_1}^{M_1}}(\Omega_1) \end{aligned}$$

where the sum runs on  $\{l_1, m_1, L_1, M_1, L_2, M_2, m'_2\}$ . We have:

$$\sum_{m_1} \overline{\mathfrak{D}_{m_1 m'_2}^{(l_1)}} \overline{Y_{l_1}^{m_1}}(\Omega_1) = \overline{\left( \sum_{m_1} \mathfrak{D}_{m_1 m'_2}^{(l_1)} Y_{l_1}^{m_1}(\Omega_1) \right)} = \overline{Y_{l_1}^{m'_2}}(\Omega'_1)$$

and by definition,  $\vec{\Omega}'_1$  is on  $Oz'$ , ( $\theta'_1 = 0$ ), so  $\overline{Y_{l_1}^{m'_2}}(\Omega'_1) = \lambda_{l_1}^{m'_2}(0) e^{-im'_2 \phi'_1}$ .

As  $\lambda_{l_1}^{m'_2}(0) = \lambda_{l_1}^0(0) \delta_{m'_2 0}$ , we obtain:

$$\langle \mathcal{N}^A(\gamma) \tilde{\xi}(\gamma) \rangle = 2\pi \sum_{\dots} \overline{b_{L_1 M_1}} b_{L_2 M_2} C_{l_1} \lambda_{l_1}^0(\gamma) \lambda_{L_2}^0(\gamma) \lambda_{l_1}^0(0) \int_{S^2} d\Omega_1 \overline{\mathfrak{D}_{M_2 0}^{(L_2)}}(\phi_1, \theta_1, 0) \overline{Y_{L_1}^{M_1}}(\Omega_1)$$



where the sum runs on  $\{l_1, L_1, M_1, L_2, M_2\}$ .

But we have:  $\mathfrak{D}_{M_2 0}^{(L_2)}(\phi_1, \theta_1, 0) = \sqrt{\frac{4\pi}{2L_2+1}} \overline{Y_{L_2}^{M_2}}(\theta_1, \phi_1)$

$$\begin{aligned} \langle \mathcal{N}^A(\gamma) \tilde{\xi}(\gamma) \rangle &= 2\pi \sum_{\dots} \sqrt{\frac{4\pi}{2L_2+1}} \overline{b_{L_1 M_1}} b_{L_2 M_2} C_{l_1} \lambda_{l_1}^0(\gamma) \lambda_{L_2}^0(\gamma) \lambda_{l_1}^0(0) \\ &\quad \times \int_{S^2} d\Omega_1 Y_{L_2}^{M_2}(\theta_1, \phi_1) \overline{Y_{L_1}^{M_1}}(\Omega_1) \\ &= 2\pi \sum_{\dots} \sqrt{\frac{4\pi}{2L_2+1}} \overline{b_{L_1 M_1}} b_{L_2 M_2} C_{l_1} \lambda_{l_1}^0(\gamma) \lambda_{L_2}^0(\gamma) \lambda_{l_1}^0(0) \delta_{L_2 L_1} \delta_{M_2 M_1} \\ &= 2\pi \sum_{\dots} \sqrt{\frac{4\pi}{2L_1+1}} \overline{b_{L_1 M_1}} b_{L_1 M_1} C_{l_1} \lambda_{l_1}^0(\gamma) \lambda_{L_1}^0(\gamma) \lambda_{l_1}^0(0) \end{aligned}$$

where the final sum runs on  $\{l_1, L_1, M_1\}$ .

Using the definition of  $\mathcal{B}_l$  (see III.14) as well as  $\lambda_l^m = \sqrt{\frac{2l+1}{4\pi}} \sqrt{\frac{(l-m)!}{(l+m)!}} P_l^m$ ,  $P_l^0 = P_l$  and  $P_l(0) = 1$ , we obtain:

$$\langle \mathcal{N}^A(\gamma) \tilde{\xi}(\gamma) \rangle = \left( \sum_{l_1} \frac{2l_1+1}{4\pi} C_{l_1} P_{l_1}(\gamma) \right) \times \left( 2\pi \sum_{L_1} (2L_1+1) \mathcal{B}_{L_1} P_{L_1}(\gamma) \right)$$

To compute  $\mathcal{N}^A(\gamma) = \int_{S^2 \times S^2} d\Omega_1 d\Omega_2 \overline{W^A(\Omega_1)} W^A(\Omega_2) \delta(\vec{\Omega}_1, \vec{\Omega}_2 - \cos(\gamma))$  we do the same computation as before with  $T(\Omega) = 1 = \sqrt{4\pi} Y_0^0(\Omega)$  so  $a_{l_1 m_1} = \sqrt{4\pi} \delta_{l_1 0} \delta_{m_1 0}$  and  $C_{l_1} = 4\pi \delta_{l_1 0}$ .

We thus obtain ( $P_0(\theta) = 1$ ):

$$\mathcal{N}^A(\gamma) = 2\pi \sum_L (2L+1) \mathcal{B}_L^A P_L(\gamma)$$

and finally:

$$\langle \tilde{\xi}(\gamma) \rangle = \left( \sum_l \frac{2l+1}{4\pi} C_l P_l(\gamma) \right) \frac{\sum_L (2L+1) \mathcal{B}_L P_L(\gamma)}{\sum_L (2L+1) \mathcal{B}_L^A P_L(\gamma)}$$

## D Computation of the angular correlation integral

### for a portion of sphere.

Let's compute the integral:

$$\begin{aligned}
I_{l'm'}^{lm}(c) &= \int_{A \times A} d\Omega d\Omega' \delta(\vec{\Omega} \cdot \vec{\Omega}' - c) Y_{l'}^{m'}(\Omega') \overline{Y_l^m}(\Omega) \\
&= \int_{S^2 \times S^2} d\Omega d\Omega' \delta(\vec{\Omega} \cdot \vec{\Omega}' - c) W^A(\Omega') W^A(\Omega) Y_{l'}^{m'}(\Omega') \overline{Y_l^m}(\Omega) \\
&= \sum_{LML'M'} \overline{b_{LM} b_{L'M'}} \int_{S^2 \times S^2} d\Omega d\Omega' \delta(\vec{\Omega} \cdot \vec{\Omega}' - c) Y_{l'}^{m'}(\Omega') Y_{L'}^{M'}(\Omega') \overline{Y_l^m}(\Omega) \overline{Y_L^M}(\Omega)
\end{aligned}$$

Using the formula of the product of two  $Y_l^m$  relative to the Clebsch-Gordan coefficients and remembering that the coefficients are real:

$$\begin{aligned}
I_{l'm'}^{lm}(c) &= \sum_{LML'M'} \overline{b_{LM} b_{L'M'}} \sum_{\lambda\mu\lambda'\mu'} \sqrt{\frac{(2l+1)(2L+1)}{4\pi(2\lambda+1)}} \sqrt{\frac{(2l'+1)(2L'+1)}{4\pi(2\lambda'+1)}} \\
&\quad \times \langle lLmM | \lambda\mu \rangle \langle lM00 | \lambda 0 \rangle \langle l'L'm'M' | \lambda'\mu' \rangle \langle l'L'00 | \lambda'0 \rangle \\
&\quad \times \int_{S^2} d\Omega d\Omega' \delta(\vec{\Omega} \cdot \vec{\Omega}' - c) Y_{\lambda'}^{\mu'}(\Omega') \overline{Y_{\lambda}^{\mu}}(\Omega)
\end{aligned}$$

The remaining integral has been computed in appendix A

$$\mathcal{I} = 2\pi \delta_{\lambda\lambda'} \delta_{\mu\mu'} P_{\lambda}(c)$$

Thus

$$\begin{aligned}
I_{l'm'}^{lm}(c) &= 2\pi \sum_{LML'M'} \overline{b_{LM} b_{L'M'}} \sum_{\lambda\mu} P_{\lambda}(c) \\
&\quad \times \sqrt{\frac{(2l+1)(2L+1)}{4\pi(2\lambda+1)}} \langle lLmM | \lambda\mu \rangle \langle lM00 | \lambda 0 \rangle \\
&\quad \times \sqrt{\frac{(2l'+1)(2L'+1)}{4\pi(2\lambda+1)}} \langle l'L'm'M' | \lambda\mu \rangle \langle l'L'00 | \lambda 0 \rangle
\end{aligned}$$

It is real and can be rewritten as integrals of three  $Y_l^m$ .

$$\begin{aligned}
I_{l'm'}^{lm}(c) &= 2\pi \sum_{LML'M'} \overline{b_{LM} b_{L'M'}} \sum_{\lambda\mu} P_{\lambda}(c) \int_{S^2} d\Omega \overline{Y_l^m}(\Omega) \overline{Y_L^M}(\Omega) Y_{\lambda}^{\mu}(\Omega) \int_{S^2} d\Omega' Y_{l'}^{m'}(\Omega') Y_{L'}^{M'}(\Omega') \overline{Y_{\lambda}^{\mu}}(\Omega') \\
&= 2\pi \sum_{\lambda\mu} P_{\lambda}(c) \sum_{LML'M'} \int_{S^2} d\Omega \overline{Y_l^m}(\Omega) \overline{b_{LM} b_{L'M'}} \overline{Y_L^M}(\Omega) Y_{\lambda}^{\mu}(\Omega) \int_{S^2} d\Omega' Y_{l'}^{m'}(\Omega') b_{L'M'} Y_{L'}^{M'}(\Omega') \overline{Y_{\lambda}^{\mu}}(\Omega') \\
&= 2\pi \sum_{\lambda\mu} P_{\lambda}(c) \int_{S^2} d\Omega \overline{W^A(\Omega) \overline{Y_L^M}(\Omega)} Y_{\lambda}^{\mu}(\Omega) \int_{S^2} d\Omega' W^A(\Omega') Y_{L'}^{M'}(\Omega') \overline{Y_{\lambda}^{\mu}}(\Omega') \\
&= 2\pi \sum_{\lambda\mu} P_{\lambda}(c) \int_{A \times A} d\Omega \overline{Y_l^m}(\Omega) Y_{\lambda}^{\mu}(\Omega) \int_{A \times A} d\Omega' Y_{l'}^{m'}(\Omega') \overline{Y_{\lambda}^{\mu}}(\Omega')
\end{aligned}$$

Remembering the  $B_{lm'l'm'}$  definitions (see section iii.2):

$$I_{l'm'}^{lm}(c) = 2\pi \sum_{LM} P_L(c) B_{LMlm} \overline{B_{LMl'm'}}$$

# Bibliography

- [Benoit et al, 2003] Benoit,A. et al (The Archeops Collaboration), A&A,399, p.L19-L23 (2003)
- [Brink et al, 1962] Brink,D.M.; Satchler,G.R., Angular Momentum (Clarendon Press 1962)
- [De Bernardis et al, 2000] De Bernardis, P., Ade, P. A. R., Bock, J. J., et al. 2000, Nature, 404, 955
- [Gòrski et al, 2005] Gòrski, K. M., Hivon, E., Banday, A. J., et al. 2005, ApJ , 622, 759 (see also <http://healpix.jpl.nasa.gov>)
- [Gradshtein et al, 1980] Gradshtein I.S.; Ryzhik,I.M.; Jeffrey,A., Table of integrals, series, and products (Academic Press 1980)
- [Hanany et al, 2000] Hanany, S., Ade, P., Balbi, A., et al. 2000, ApJ , 545, L5
- [Hivon et al, 2002] Hivon et al, The Astrophysical Journal, Volume 567, Issue 1, pp. 2-17 (2002).
- [Masi et al, 2006] S.Masi, et al. 17th ESA Symposium on European Rocket and Balloon Programmes and Related Research, 30 May-2 June 2005, Sandefjord, Norway. ESA Publications Division, ISBN 92-9092-901-4, 2005, p 581-586.
- [Messiah, 1964] Messiah,A. mécanique quantique Tome 2 (Editions DUNOD, paris 1964)
- [Natoli et al, 1997] P. Natoli, P.F. Muciaccia, and N. Vittorio, ApJ Letter 488, L63 (1997).
- [Seljak et al, 1996] Seljak, U., Zaldarriaga, M., 1996 ApJ, 469, 437 (see also <http://www.cmbfast.org>)
- [Tegmark, 1997] Tegmark, M. 1997, PrD , 56, 4514
- [Wandelt et al, 2001] Wandelt et al, Physical Review D (Particles, Fields, Gravitation, and Cosmology), Volume 64, Issue 8, 15 October 2001
- [Zaldarriaga et al, 2000] Zaldarriaga, M., Seljak, U., 2000 ApJS, 129, pp 431-434